Spring 5-2012

Molecular Network Development of a Thermosetting Epoxy-Amine Polymer

Christopher Michael Sahagun
University of Southern Mississippi

The University of Southern Mississippi

MOLECULAR NETWORK DEVELOPMENT OF A THERMOSETTING EPOXY-AMINE POLYMER

by

Christopher Michael Sahagun

Abstract of a Dissertation
Submitted to the Graduate School
of The University of Southern Mississippi
in Partial Fulfillment of the Requirements
for the Degree of Doctor of Philosophy

May 2012

ABSTRACT

MOLECULAR NETWORK DEVELOPMENT OF

A THERMOSETTING EPOXY-AMINE POLYMER

by Christopher Michael Sahagun

May 2012

Epoxy-amine resins find wide application as the matrix material of high performance polymer composites due to their favorable mechanical properties, thermal properties and solvent stability. These properties are derived from the complicated, highly crosslinked molecular network that is characteristic of these thermoset polymers. The connectivity of the molecular network has a strong influence on the physical performance of the finished part. Non-homogeneity in the network structure can degrade these favorable properties through the introduction of low-energy pathways for solvent penetration or fracture propagation. This work examines nanoscale variation in the crosslink density of the epoxy-amine network. Specific attention is paid to the influence of cure temperature on the network-building reaction and the subsequent effect on the architecture of the crosslinked molecular network. Thermal, rheological and spectroscopic techniques are used to monitor key chemical and structural changes during network growth. Atomic force microscopy is used to understand nanoscale fracture behavior in terms of the low energy pathways that result from a non-homogeneous distribution of crosslink density. The influence of processing-induced changes in molecular connectivity is discussed in terms of observed nanoscale morphology and fracture properties of the cured material.

The University of Southern Mississippi

MOLECULAR NETWORK DEVELOPMENT OF A THERMOSETTING EPOXY-AMINE POLYMER

by

Christopher Michael Sahagun

A Dissertation
Submitted to the Graduate School
of The University of Southern Mississippi
in Partial Fulfillment of the Requirements
for the Degree of Doctor of Philosophy

Approved:

_____Sarah Morgan_____
Director

_____Sergei Nazarenko_____

_____James Rawlins_____

_____Daniel Savin_____

_____Jeffrey Wiggins_____

_____Susan A. Siltanen_____
Dean of the Graduate School

May 2012

ACKNOWLEDGMENTS

I gratefully acknowledge the unconditional support provided to me by my major research advisor, Dr. Sarah Morgan, and I am especially grateful for the countless opportunities she provided for me as her student.

I also wish to extend my gratitude to my doctoral committee, Dr. Sergei Nazarenko, Dr. James Rawlins, Dr. Daniel Savin, and Dr. Jeffrey Wiggins. I would also like to thank Diane Rawlings, Stephen Christensen and Terry Schneider from The Boeing Company for helpful advice regarding the needs of the aerospace community.

I would also like to acknowledge the contribution of Katrina Knauer who spent an entire summer with me analyzing data from rheological experiments.

Additionally, I wish to thank the Office of Naval Research as the primary funding source for this research through award number N00014-07-105 as well as the National Science Foundation for providing me with financial support through Igert award 0333136.

TABLE OF CONTENTS

LIST OF TABLES

Table

LIST OF ILLUSTRATIONS

Figure

CHAPTER I

INTRODUCTION

This work is an investigation into the development of the crosslinked molecular network of the diglycidyl ether of bisphenol A when cured with 3,3'-diaminodiphenyl sulfone. This resin system is typical of the type used industrially as the polymeric matrix of high performance carbon fiber reinforced composite structures. This work is primarily focused on monitoring the development of sub-one hundred nanometer structure during the initial stages of cure in order to draw conclusions about the architecture of the cured network and the influence of processing conditions on network development.

The importance of the architecture of crosslinked molecular networks in the determination of bulk physical properties is well known.[1-3] One major goal of current research in thermoset networks is the reconciliation of molecular scale parameters with bulk scale properties. This research interest is driven by a desire to predict final part performance from knowledge of molecular scale characteristics. [4, 5] This type of approach to materials research is naturally attractive as the ability to predict macroscopic performance from molecular scale parameters will reduce material development time and costs as well as provide the opportunity to engineer part performance from the molecular scale. Various strategies have been developed to correlate molecular characteristics to macroscopic behavior, however the computational modeling of polymer networks is generally accepted as the most powerful method.[5-8] The accuracy of any attempt to scale molecular characteristics to bulk properties hinges on ensuring that the model network reflects the true structure of the real network. A full understanding of the structure across multiple scales, therefore, is necessary to ensure the accurate reproduction of a real

system with any property-scaling model. These scales range in size from a few angstroms to a few millimeters. For example, angstrom-scale structure is important when considering the influence of different structurally isomeric monomers. Structure on the scale of a few tens of nanometers, the scale investigated in this work, is important when considering connectivity within the molecular network. Structure at the micrometer scale is important when considering the influence of interphases between the matrix and the reinforcing material. And finally, scales of a few millimeters and larger are investigated when considering the influence of the dimensions and orientation of the reinforcement phase.

These scales provide a sort of "pathway" that link the most fundamental component of a composite part's structure, the constitution of the individual monomer molecules, up to the characteristic that matters most, the observable performance of the finished part. A significant amount of research effort has been expended to provide the knowledge that makes this pathway useful. Molecular scale characterization techniques have provided valuable information about the influence of the structure and motions of crosslinked epoxy networks at the angstrom and nanometer scale.[9-13] Bulk mechanical analysis of composite test coupons has provided information about the relationship between structure and part performance at the micron to millimeter scale.[14-16] These studies have shown that attempting to predict macroscopic performance from molecular characteristics is a promising area of research that is worthy of pursuit. The present work seeks to add knowledge to this multiscale research strategy by revealing the structure of epoxy-amine networks at the mesoscale. This document presents the results of an investigation into the development of substructure within the molecular network at the

scale of 40-100 nanometers and demonstrates that this architecture can be controlled by the processing temperature of the epoxy-amine system.

The results of this work will enhance the utilization of economically important epoxy-amine thermosets by providing information that will improve the ability to predict bulk performance from molecular characteristics. Recently, the increased use of composite materials for aerospace and marine applications has become a significant driving factor for this type of composite matrix research. Thermoset polymers such as the epoxy-amine system studied here are an attractive choice for use in demanding environments due to their durability, inherent corrosion resistance and relative ease of processing. The recent delivery of Boeing's 787 (of which a significant portion of the airframe is made up of carbon fiber/epoxy composite materials) as well the current production of the US Navy's new Zumwalt class destroyer (with a carbon fiber/vinyl ester deck and deckhouses) demonstrate the continuing interest of using reinforced thermoset materials for the production of high profile, large scale industrial projects.[17, 18]

In addition to use as structural materials, epoxy systems also find application as adhesives, coatings and as a protective encapsulant for electronic equipment. Epoxy based chemical systems will continue to be an economically important class of materials for years to come due to their relatively low cost to property ratio. The versatility and economic importance of epoxy-based systems is underscored by the fact that the world-wide total market based upon epoxy chemicals is expected to be worth over 17 billion US Dollars in 2012.[19]

Current Limitations in the Understanding of Structure/Property Relationships in Epoxy-amine Crosslinked Molecular Networks

The current understanding of structure in epoxy-amine molecular networks at the mesoscale is not as well developed as at other scales. The development of scaling models for thermoset systems, therefore, will be enhanced by additional information regarding the network structure at this scale. Non-homogeneity in the structure of epoxy-amine networks at the scale of tens of nanometers has long been suspected, but information regarding the nature and development of this non-homogeneity is limited. This work adds to the available literature regarding the structure of epoxy-amine systems at these dimensions.[20, 21]

Generally, research regarding the structure/property relationships of thermoset networks involves the synthesis of multiple crosslinked networks consisting of different structural isomers and then comparing the macroscopic performance qualities of the material. This research approach has been quite fruitful, however, the analysis of these results is typically premised upon the assumption of the formation of a continuously homogeneous three dimensional network. Any non-homogeneity in the network will necessarily introduce a degree of uncertainty when considering how to scale molecular scale parameters to bulk properties. This uncertainty is a consequence of the fact that in a non-homogeneous network, not all regions of the material will be identical – some regions will be topologically different. Therefore, a decision must be made as to which region of the crosslinked network should be used as the basis for scaling a property across orders of magnitude of size. Often, an "average" description of the network is assumed. An example of this averaging process is the classical prediction of tensile

strength for a crosslinked material. Bueche calculated that the maximum stress capable of being supported by a crosslinked polymer is given by the following relationship: [22, 23]

$$\sigma_B \propto \left[1 - \frac{2\overline{M_c}}{\overline{M_N}}\right]^{2/3} \quad (1)$$

where σ_B is the stress at break and $\overline{M_c}$ and $\overline{M_N}$ are the average molecular weight between crosslinks and the number average molecular weight, respectively. Nonhomogeneity in the distribution of crosslinks within the network, however, leads to uncertainty as to which region should be defined as possessing the "true" molecular weight between crosslinks. Generally, the value of $\overline{M_c}$ is estimated by the following relationship:[24]

$$G' = \frac{RT\rho}{M_C} \quad (2)$$

where R is the gas constant, T is the absolute temperature, ρ is the density and G' is the storage modulus. The value for storage modulus is empirically determined, usually through dynamic mechanical analysis or rheometrically. However, these are bulk characterization techniques that are unable to truly resolve molecular scale variation in the crosslink density. The value for M_c provided by dynamic analysis is best considered to be an average value. This means that the value of σ_B calculated in Equation 1 is dependent on a value averaged over the entire sample. This type of analysis will lead to an overestimation of the maximum stress as it is based upon knowledge of the average network structure as opposed to the "weakest link" of the network – in this case the region with the lowest amounts of strong covalent bonds available to resist fracture propagation. For fracture propagation, the region of the non-homogeneous network with the lowest amount of crosslinking will serve as what can be termed the "property-critical" region of the network architecture. As this region possesses fewer strong crosslinks, it is

reasonable to expect that it will also present a lower barrier to propagation of the crack tip. The physical properties of this phase of the non-homogeneous network, therefore, will contribute strongly to the determination of the maximum tensile strength of the crosslinked network. If regions of relatively lower crosslink density form a continuous path through the sample, even if this phase is only a small fraction of the overall network, this region will have a disproportionately strong influence on the ability for a crack tip to move through the molecular network and cause part failure.

A similar concept is illustrated in Figure 1 for the case of the penetration of a water molecule into a model thermoset network. The illustration on the left shows a model of a perfectly homogeneous network while the right shows a network with a non-homogeneous distribution of crosslinking. The homogeneous network presents no preferred pathway for transport of the water molecule as all areas are similarly crosslinked. The non-homogeneous network, however, has a low energy pathway that results from a connected region of lower crosslink density. Although this region is only a fraction of the total network, it would be expected to strongly influence the ability of the network to resist penetration of small molecules into the network. Any attempt to predict the solvent penetration properties in this type of network should base the predictive model on the network structure in this small, property-critical region.

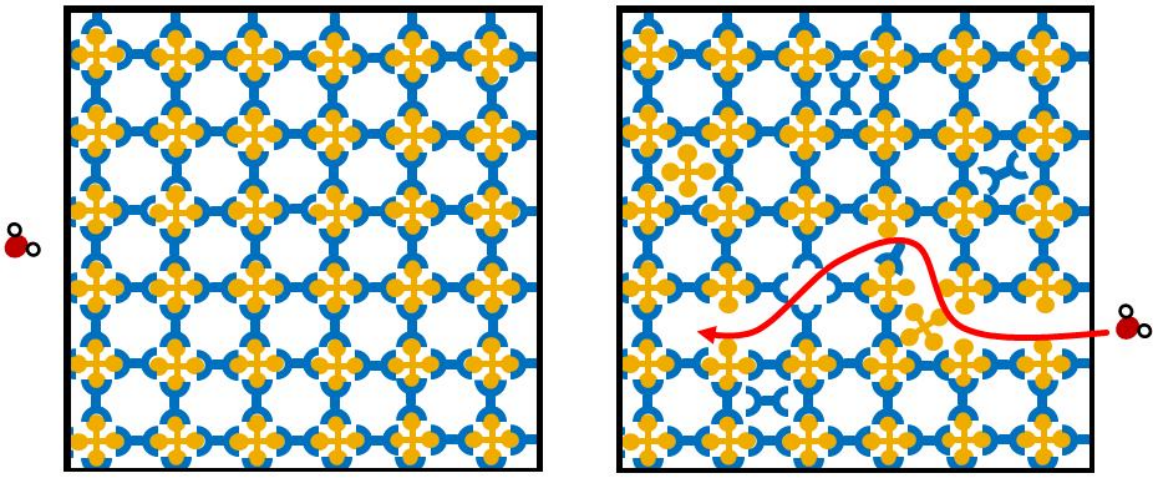

Figure 1. Model homogeneously (left) and non-homogeneously (right) networks. Non-homogeneity in the network architecture presents a low energy pathway for mass transport.

Understanding the nature and development of this property-critical region within a crosslinked epoxy-amine network is important for enhancing the ability to reliably predict macroscopic properties from molecular scale parameters. This work investigates the formation and distribution of heterogeneous regions of crosslink density within the epoxy-amine network. Additionally, a means to control connectivity within the network during the initial stages of processing is described.

Research Strategy

Highly crosslinked epoxy-amine networks such as the Epon 828/3,3'-diamino diphenyl sulfone system studied here have a notoriously intractable nature.[25] The crosslinked structure that lends itself to the favorable physical properties that make these systems an attractive choice for demanding applications also makes characterization of the network structure difficult. To get around the difficulties of characterizing the fully cured network, this work instead monitors the growth of the molecular network during the network building reaction. Particular emphasis was placed on the use of atomic force

microscopy to monitor the development of nanostructure in the curing system as it transitions from low molecular weight monomer to a highly crosslinked, three dimensional network. Samples in different states of network development were fractured in order to use the propagating crack tip as a nanoscale "probe" to reveal variation in the crosslink density. This will be discussed in much greater detail in a subsequent section. Chemical changes in the curing system were monitored with real-time near-infrared spectroscopy. Near-infrared spectroscopy is able to resolve the relative concentration of primary amines and secondary amines and consequently allows the concentration of tertiary amine to be calculated. As will be shown, this type of analysis reveals the general structure of molecular segments (that is, linear or branched) as a function of cure time, providing valuable information about the underlying molecular structure of the observed morphology in the developing network. And finally, fracture testing was performed in order to understand the relationship between nanoscale morphology, network structure and bulk fracture properties.

The overall strategy adopted by this work is to start with the broadest understanding of the relationship between cure time and the state of network development and then to refine this description with knowledge gained from higher-resolution characterization techniques. The general strategy of this work can be outlined as follows:

1. Determine if a crosslinked molecular weight network is present, and if it is, determine if it is still growing (rheometry, differential scanning calorimetry).
2. Determine what fraction of the sample is crosslinked and what fraction is not (near-infrared spectroscopy).

3. Determine how evenly distributed the crosslinks are within the molecular network (atomic force microscopy).

Characterizing the growth of the network in this way at successively longer amounts of cure time allows the growth of the molecular network to be tracked. Repeating this type of characterization at successively higher temperatures allows the influence of cure temperature on the way monomer is added to the network growth to be determined.

CHAPTER II

THE EPOXY-AMINE MOLECULAR NETWORK

Chapter Overview

This chapter provides a general overview of epoxy-amine molecular networks. This chapter includes a discussion of the term "network architecture" as used in this work, a description of the industrial processing techniques used to produce epoxy-amine networks in fiber reinforced composite materials and an overview of the polymerization reaction of multifunctional epoxies and amines with specific attention paid to the potential for etherification reactions as well as a description of the complicated kinetics of the polymerization reaction. This section concludes with a discussion of the time-temperature transformation behavior of epoxy-amine systems during the network building reaction and a review of models of thermoset network formation.

Architecture of Epoxy-Amine Molecular Networks

Epoxy-amine thermoset polymers derive their favorable properties from their crosslinked molecular network. A convenient way to frame a discussion of structure/property relationships in crosslinked polymers is to discuss the structure in terms of the "network architecture" of the system. Network architecture can refer to a few different structural aspects of the crosslinked molecular network. For example, networks built from different epoxy and amine monomer species will yield different molecular network architectures. Consider two different epoxy-amine networks, one built from 3,3'-diaminodiphenyl sulfone and another built from 4,4'-diaminodiphenyl sulfone. These networks will have different network architectures due to the difference in the position of the reactive amine on each structurally isomeric monomer species. As another example, networks built from epoxy prepolymers with different molecular

weights will yield molecular networks with different architectures as each network will have a different molecular weight between crosslinks. These examples show that the architecture of the molecular network can be tuned through judicious choice of monomer species. In fact, research into the influence of this type of network architecture has been an active area of research for many years. Selected results will be briefly summarized in a subsequent section to illustrate the influence of molecular scale characteristics on bulk properties.

This work uses the term "network architecture" in a slightly different way. Here, the term network architecture refers to *connectivity* within the crosslinked molecular network. This qualification is subtle, but important. For this work, connectivity within the network should be understood as a description of how well connected one region of the network is to another region through strong covalent bonds. Molecular networks can, in general, be classified as possessing one of two different types of architectures – a homogeneously connected network architecture or a non-homogeneously connected architecture. The homogeneity of the molecular network architecture is defined by the distribution of crosslinks in the volume of the sample. A homogenously connected molecular network will show the same number of crosslinks in all regions of the sample while a non-homogenously connected molecular network will show domains with different crosslink densities.

As discussed in the introduction, non-homogeneity in the distribution of crosslink density of the system will be expected to influence pathway dependent properties such as solvent penetration and fracture propagation. Covalent bonds act as a barrier to the transport of mass or to the propagation of a crack tip. The non-homogeneous network

depicted in Figure 1 contains a pathway consisting of a continuous region of relatively lower crosslink density that facilitates the penetration of the water molecule into the network. (It is important to note that this scheme only demonstrates physical processes and not chemical processes such as the influence of secondary bonding on transport properties. Regardless, this simple scheme is still applicable as, regardless of the role of secondary bonding, no transport can occur if the pathway is blocked by covalently bonded material and free volume is not available to enable mass transport.) A similar effect will also influence fracture propagation. The relatively higher concentration of covalent bonds in some regions present a barrier to fracture propagation which will cause the propagating crack tip to deviate in order to follow the lowest energy pathway. That is, the propagating crack tip will preferentially travel through regions of relatively lower crosslink density. As will be seen, this type of fracture behavior through non-homogeneously connected networks is a fundamental aspect of this research.

The Industrial Production of Epoxy-Amine Molecular Networks

Polymerization is usually thermally induced during the processing of the epoxy-amine systems used as composite matrices for high performance aerospace applications. Modification of the thermal cycle during processing, therefore, provides an opportunity to influence network assembly and, consequently, the resulting molecular architecture of the fully-cured system. Improving the ability to control network architecture provides an attractive opportunity to tune the physical properties of composite matrices from the molecular scale. This has clear benefits for optimizing performance as well as potentially enabling the composite matrix to perform multiple functions. For example, controlling the distribution of free volume within the crosslinked molecular network can provide

improved solvent or water resistance thereby allowing the finished part to perform dual roles as a structural member and a moisture barrier, reducing both weight and fabrication complexity.

Epoxy-amine systems used for composite part production typically undergo a significant amount of processing before the part is put in a mold and cured. These initial processing steps must be considered in any attempt to control the architecture of the molecular network in an industrial environment. Prior to the polymerization reaction, the epoxy-amine system is either a relatively low viscosity liquid or can be heated to yield a relatively low viscosity liquid. This low viscosity allows the resin to "wet out" the reinforcement phase. The resin is usually introduced into the reinforcement phase in one of two ways, each taking advantage of the low viscosity of the epoxy-amine system at low stages of cure. The resin can be pre-impregnated into the fiber ("pre-preg"), usually at a dedicated pre-preg facility separate from the part manufacturer and then stored until part fabrication. Since the initiation of cure must be delayed, pre-pregged fibers must be stored at a temperature low enough to delay cure until part fabrication. The handling characteristics of the material can be tuned through a process called B-staging where polymerization is driven to some intermediate stage between uncured monomer and a fully cured network. Generally, B-staging will be done to raise the glass transition temperature to somewhere between the storage temperature and the lay-up temperature to prevent resin from flowing during storage but allowing the pre-preg to take the shape of a mold during lay-up. This type of fabrication technique is typical for aerospace structures that require low void content.

Alternatively, reinforcing fibers can be impregnated with resin through a technique known as vacuum assisted resin transfer molding (VARTM). The epoxy and amine curing agent are mixed immediately prior to part fabrication with attention paid to pot-life of the material – the time until the curing reaction has driven conversion far enough that the system no longer has a processable viscosity. A vacuum pump is used to draw resin from the pot into the fiber matte that has been previously laid onto the mold and encased in a vacuum bag. This also allows atmospheric pressure to compress the part, thereby reducing void content. This type of fabrication technique is typically used to create very large composite structures where it is unfeasible to use an autoclave. For large structures, room-temperature curing resin systems are used, although smaller parts can also be cured in an autoclave just as pre-pregged materials.

These fabrication techniques introduce some degree of cure during processing. As will be shown through the results of this work, it is these initial stages of resin cure that appear to have the largest influence on the final network structure. It is important to understand that consistent handling during this initial wet-out phase of part fabrication is required to ensure consistent performance of the finished part.

The Epoxy-Amine Network Building Reaction

Epoxy-amine systems develop a highly crosslinked molecular network through a step growth polymerization reaction of multifunctional monomers. The curing reaction is quite complex due to the evolution of both the chemical environment and the physical environment of the system during the network building reaction. It is reasonable to anticipate that this complexity may contribute to the development of a non-homogeneous network structure.

This work will focus on the well-known epoxy system consisting of the diglycidyl ether of bisphenol A (Epon 828) cured with 3,3'-diaminodiphenyl sulfone. The structure of each monomer is shown in Figure 2.

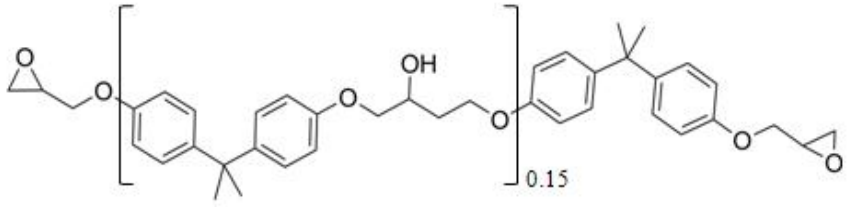

diglycidyl ether of bisphenol A

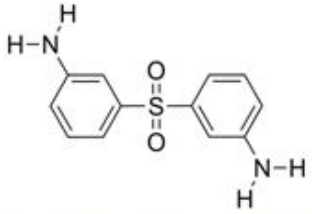

3,3'-diaminodiphenyl sulfone

Figure 2. Molecular structure of the diglycidyl ether of bisphenol-A (Epon 828) and 3,3'-diaminodiphenyl sulfone.

Epon 828 is difunctional while the 3,3'-diaminodiphenyl sulfone curing agent is tetrafunctional. The tetrafunctionality of the curing agent allows the system to develop crosslinks and therefore to form an infinite molecular weight network. It is important to notice that two of the reactive species (the labile hydrogen atoms) on the tetrafunctional curing agent are located on the same nitrogen atom. The effect of this is that the reactive amine is essentially two different species during the chemical reaction. For this work, the monomer was mixed in a 1:1 stoichiometric ratio by reactive groups. This was done so that, theoretically, the system could be cured to 100% conversion of the reactive groups

and to minimize the development of etherification-induced linkages at late stages of the reaction.

The polymerization process proceeds through the ring opening reaction of the epoxy moiety by the aromatic amine.[26] Other reactions that contribute to the overall network architecture, however, are also possible. The network building reaction may proceed by etherification of the oxirane by reaction with a hydroxyl group. Additionally, it is possible for the epoxy to self-polymerize, however this reaction requires appropriate catalysis and therefore will not be considered here.[27-30] Figure 3 shows what are generally considered to be the most important network building reactions.[25] Figure 3a shows the first step of the network building reaction – the reaction of an epoxy group with a primary amine. This reaction produces a linear segment. Figure 3b shows the reaction of a secondary amine with an epoxy group to produce a branch or a crosslink, depending on the prior connectivity of the participating species. Figure 3c shows the etherification of an epoxy group by a hydroxyl moiety.

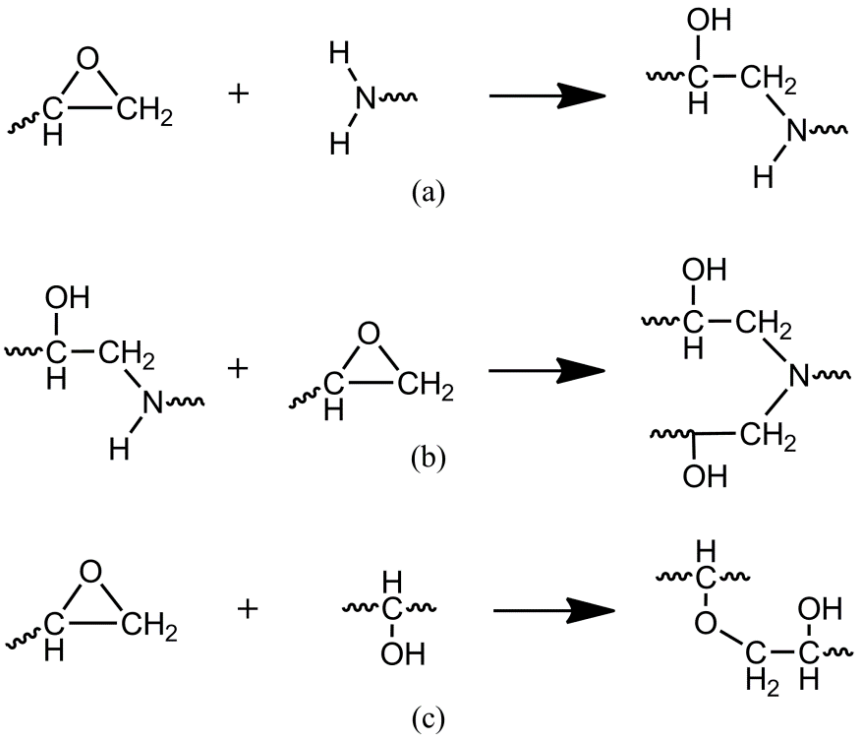

Figure 3. Epoxy-amine network-building reactions. (a) reaction of the epoxy with a primary amine. (b) reaction of the epoxy with a secondary amine. (c) etherification reaction.

The reaction between the aromatic amine and epoxy group is the major network-building reaction in the development of epoxy-amine molecular networks.[26, 31] Each amine has two labile hydrogen atoms and each of these atoms is capable of participating in the ring opening reaction. The primary amine is generally considered to be more reactive toward the epoxy group.[29, 32] This will be discussed in more detail shortly.

Autocatalytic behavior has been observed in the epoxy/amine reaction. This behavior results from the stabilization of the participating species immediately prior to reaction.[33] The hydroxyl group forms a temporary hydrogen bond with the oxygen in the epoxy ring, thereby stabilizing the molecule for nucleophilic attack by the amine curing agent. The ring-opening reaction produces a hydroxyl group as shown in Figure 3, so this autocatalytic behavior becomes increasingly important with conversion up until the

point where the system becomes diffusion restricted some time after gelation. The catalytic nature of the hydroxyl species has been successfully utilized to explain observed conversion behavior of glycidyl ether resins cured with 4,4'-diamino diphenyl sulfone.[33]

While likely present in small quantities, crosslinks resulting from the etherification reaction of the oxirane ring with a hydroxyl group make only a minor contribution to the overall molecular network structure. The reaction of an epoxide with a hydroxyl group is considered to have a higher activation energy than the reaction of an epoxide with an aromatic amine and therefore is less favorable.[33] Studies of a model system consisting of monofunctional 1,2-epoxy-3-phenyoxypropane cured with 4,4,'-diaminodiphenyl sulfone showed that the etherification reaction generally occurs after extended cure times at elevated temperatures and during the late stages of reaction in systems with excess epoxy.[34, 35] A study of a model phenylglycidyl ether molecule with various amine species found a negligible reaction between the epoxy and hydroxyl groups produced during the reaction.[36] In other studies, no etherification reaction was detected in the polymerization of an aromatic amine with 4,4'-diaminodiphenyl sulfone.[33, 37] When the etherification of the epoxy group by a hydroxyl group does occur, it has the predictable effect of reducing the overall amine conversion and also causes gelation of the system at lower levels of epoxy conversion.[38, 39]

Crosslinking due to etherification becomes more likely in systems with excess epoxy, systems cured at elevated temperatures and systems cured for extended periods of time. The cure system and conditions studied as part of this research do not meet these criteria, so etherification-induced crosslinks are not thought to contribute heavily to the

overall molecular network structure. Regardless, the possible development of these molecular network connections is noted.

The Complex Chemical Kinetics of the Network Building Reaction

The chemical kinetics of the epoxy-amine network forming reaction are complicated by the number of different species involved in the reaction, the autocatalytic nature of the ring-opening reaction and by the changing concentrations of these species during the network building reaction. The complexity of the reaction becomes clear when attempting to formulate a rate equation to describe the consumption of epoxy groups:[25, 29, 34, 40, 41]

For the uncatalyzed reaction of epoxy with primary amine;

$$-\frac{d[E]}{dt} = k_{1^0}^{0}[E][A_{1^0}] \tag{3}$$

where $[E]$ is the concentration of epoxy groups, $k_{1^0}^{0}$ is the rate constant for the uncatalyzed reaction of epoxy with primary amine, and $[A_{1^0}]$ is the concentration of primary amine.

For the uncatalyzed reaction of epoxy with secondary amine;

$$-\frac{d[E]}{dt} = k_{2^0}^{0}[E][A_{2^0}] \tag{4}$$

where $k_{2^0}^{0}$ is the rate constant for the uncatalyzed reaction of epoxy with secondary amine and $[A_{2^0}]$ is the concentration of secondary amine.

For the catalyzed reaction of epoxy with primary amine;

$$-\frac{d[E]}{dt} = k_{1^0}[E][A_{1^0}] \tag{5}$$

where k_{1^0} is the rate constant for the catalyzed reaction of epoxy with primary amine.

For the catalyzed reaction of epoxy with secondary amine;

$$-\frac{d[E]}{dt} = k_{2^0}[E][A_{2^0}] \quad (6)$$

where k_{2^0} is the rate constant for the catalyzed reaction of epoxy with secondary amine.

For the etherification reaction, where appropriate;

$$-\frac{d[E]}{dt} = k_{OH}[E][OH] \quad (7)$$

where k_{OH} is the rate constant for the etherification reaction and $[OH]$ is the concentration of the hydroxyl catalyst.

These rate equations yield an overall rate equation;

$$-\frac{d[E]}{dt} = k_{1^0}^{0}[E][A_{1^0}] + k_{2^0}^{0}[E][A_{2^0}] + k_{1^0}[E][A_{1^0}] + k_{2^0}[E][A_{2^0}] + k_{OH}[E][OH] \quad (8)$$

This kinetic scheme involves a series of coupled reactions. For example, the concentration of hydroxyl groups is coupled to the conversion of epoxies while the concentration of secondary amine is coupled to the conversion of primary amine and the rate constants of the catalyzed reactions are tied to the concentration of hydroxyl groups. This severely complicates the determination of a solution to the overall rate equation.

Efforts have been made to simplify the kinetic treatment of epoxy-amine curing reactions by neglecting both the uncatalyzed reaction and the etherification reaction,[42] by assuming equal reactivity of the primary and secondary amine,[43] and by fitting rate equations to empirical data.[44-46] These simplifications, however, have been criticized as oversimplifying the kinetics of the reaction and consequently have found their most appropriate application as a means of quality control and *in situ* monitoring of the cure progress.[25]

Fortunately, for the purposes of the present work, valuable information about the state of the network can still be obtained without the elucidation of a precise rate

equation. Here, the *relative rate of production* of secondary and tertiary amine species is sufficient to understand the influence of chemical kinetics on the resulting structure of the crosslinked molecular network. This will be discussed further in the section concerning use of near-infrared spectroscopy to elucidate the average segmental structure of the developing crosslinked network.

Influence of Temperature on the Epoxy/Amine Reaction

Consider the catalytic effect of the hydroxyl moieties discussed previously.[33, 36] Hydroxyl groups function as a catalyst for the network building reaction by increasing the pre-exponential factor of the reaction by stabilizing the participating molecules in a configuration favorable for the reaction of the epoxy group with the amine. It follows, then, that the catalytic behavior is most effective when the hydroxyl group is in close proximity to the reaction site. In this way, the hydrogen bond can essentially "hold" the two participating species together until the reaction occurs. This means that the influence of catalysis by the hydroxyl group is likely more important for the reaction of the secondary amine rather than the primary amine. The reason for this is shown in Figures 4a-b. Figure 4 shows energy minimized space filling (van der Waals radii) models of Epon 828/3,3'-DDS chains obtained from a simple molecular dynamic simulation. The conformation and position of the atoms is representative of what would be expected of the chain in unreacted monomer (although monomer is not shown here). One labile hydrogen atom on the aromatic amine is shown highlighted in green. Figure 4a shows the expected conformation of the chain end of a primary amine. There is no adjacent hydroxyl group nearby to produce a catalytic effect. There will be hydroxyl groups present on monomer species (see Figure 2) and on other chain ends in the area, however

these species are not able to “hold” the participating species together for the reaction to occur. Figure 4b shows the expected conformation of a secondary amine, again, with a labile hydrogen atom shown highlighted in green. This reactive site now has an adjacent hydroxyl group, as it has undergone reaction with an epoxy group. This adjacent hydroxyl group is available to perform a catalytic role as it is in close proximity to the reactive site and is therefore able to stabilize nearby monomer to increase the likelihood of the reaction. In this way, the catalytic effect of hydroxyl species is more important for the secondary amine reaction as compared to the reaction of the primary amine. In terms of influence on the developing architecture, this means that the autocatalytic behavior is more likely to encourage the production of branches or crosslinks that result from the reaction of the secondary amine. Hydrogen bonding tends to be disrupted at elevated temperatures, therefore, the autocatalytic behavior has a degree of temperature dependence to it with the autocatalytic effect becoming diminished at temperatures above around 100°C.

The implications of this behavior for structure development, therefore, are that the autocatalytic behavior should favor the production of branched/crosslinked segments at a rate more near to that of the rate of production of linear segments when the reaction occurs at low temperatures. There is, of course, a limit to this effect as the higher activation energy required for the reaction of a secondary amine with an epoxy group will become influential as the amount of thermal energy in the system decreases at lower reaction temperatures.

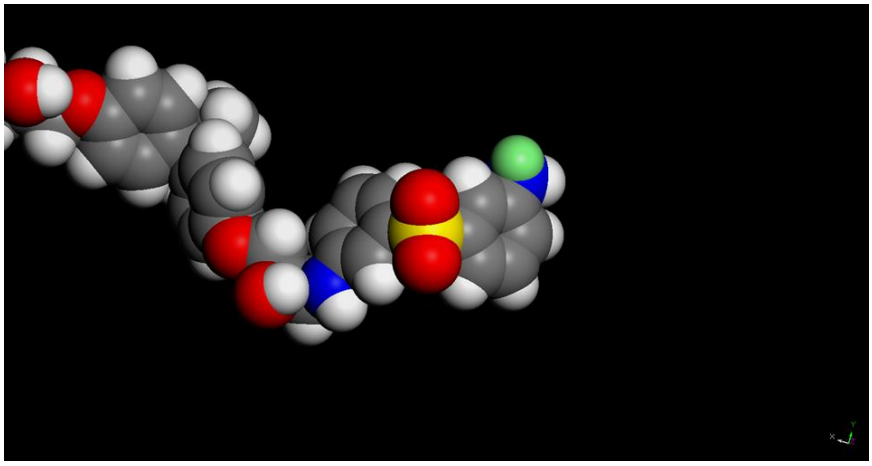

(a)

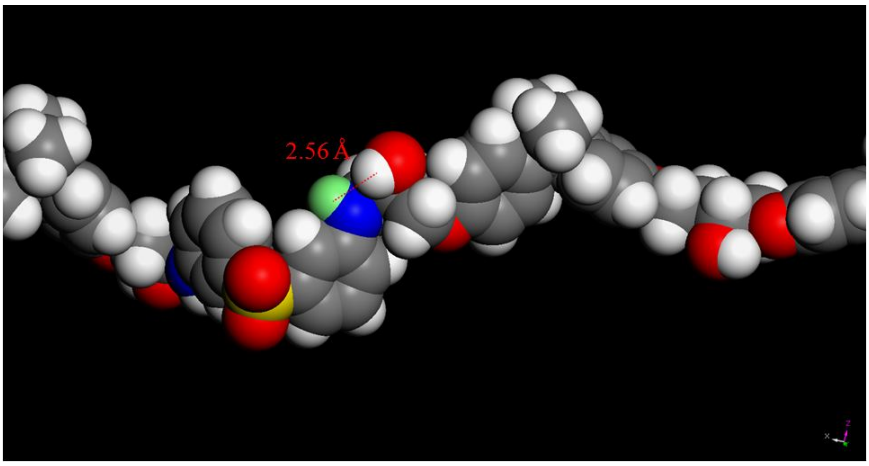

(b)

Figure 4. Space-filling model of Epon 828/3,3'-DDS showing primary amine (4a) and secondary amine (4b).

Primary and secondary amines have been shown to have different reactivities in the network building epoxy-amine reaction.[29, 32, 47] Like the autocatalytic behavior, the reactivity ratio of the primary amine to the secondary amine is also temperature dependent. Kinetic analysis of the influence of cure temperature on the reactivity ratio of these species has shown that while primary amines are more reactive with epoxies at all temperatures, the difference in the reactivity ratio is less at elevated temperatures.[47] The implications of this behavior for structure development, therefore, is that the production

of branched/crosslinked segments should occur at a rate more near to that of the rate of production of linear segments when the reaction occurs at elevated temperatures. This is in contrast to the influence of the autocatalytic behavior, which encourages the production of branched/crosslinked segments at lower temperatures. These effects indicate that there should be a temperature range somewhere between these two influences that encourages the production of linear structure much faster than the production of branched/crosslinked structure. As will be shown, this behavior, in fact, seems to be a major influence on the initial structure development of the Epon 828/3,3'-DDS system. This temperature-dependent behavior was exploited in the present work to tune nanostructure formation in the developing network.

Segment Structure as an Indicator of Network Architecture

The previous discussion made special effort to distinguish between primary and secondary amine species. The reason for this is that knowing the relative concentration of each species provides information about the state of the crosslinked network. Primary amines react with a single epoxy unit to yield a secondary amine. This reaction produces a linear segment. A high relative concentration of secondary amine, therefore, indicates that the network is largely linear. This secondary amine then goes on to react with another epoxy unit to yield a tertiary amine. Tertiary amine is indicative of a branch or crosslink. A high concentration of tertiary amine, therefore, indicates highly crosslinked architecture. Near infrared-red spectroscopy is capable of discriminating between primary and secondary amine (and the concentration of tertiary amine can be calculated from the balance of these groups). As will be seen, this is a powerful technique for understanding the "average" molecular connectivity of the growing molecular network.

Time-Temperature Transformation Behavior of Thermosetting Networks

The change in the characteristics of the epoxy-amine sample that occur as it transitions from low molecular weight monomeric and oligomeric material to a crosslinked molecular network is referred to as the transformation behavior of the system.[48] Generally, the transformation behavior of the system is studied as a function of both the reaction temperature and the reaction time in order to characterize the time-temperature transformation (TTT) behavior of the system.

Characterizing the time-temperature transformation behavior of the curing epoxy-amine system reveals the structure of the developing network during different stages of the network-forming reaction. The state of the network at different cure temperatures can be plotted at increasing cure times to produce a time-temperature transformation diagram.[49] Figure 5 shows a typical time-temperature transformation diagram of a thermosetting polymer. Time-temperature transformation diagrams show the length of reaction time required to reach some stage of network development at a given temperature. In this way, the time-temperature transformation diagram serves as a "road map" for the production of samples with some desired state of network development. This type of analysis is valuable for the production of samples with some known state of molecular network development.

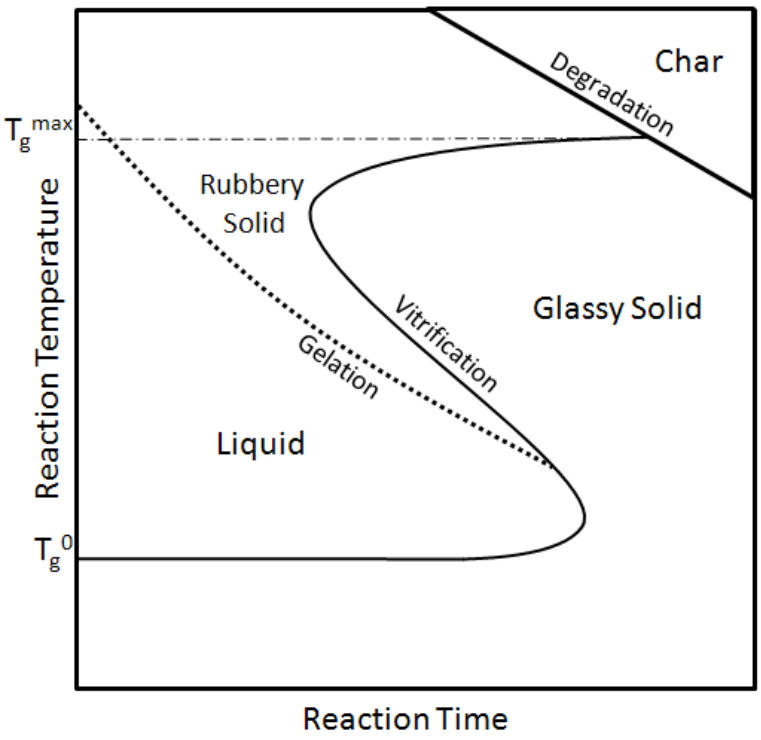

Figure 5. Theoretical time-temperature transformation diagram of a thermosetting polymer illustrating the reaction time required to reach various states of network structure at different reaction temperatures. T_g^0 is the glass transition temperature of the uncured resin. T_g^{max} is the maximum attainable T_g of the resin system.

Characterization of the time-temperature transformation behavior of the system hinges upon knowing the time required to reach two key stages of network growth as a function of the reaction temperature: gelation and the onset of vitrification. The gel point marks the initial appearance of a sample-wide molecular network while the onset of vitrification marks the shift of the network building reaction from chemical to diffusion control. Each event has important implications for the architecture of the developing molecular network. These points can be identified by monitoring the ratio of the loss modulus to the storage modulus (that is, the tan δ) and the glass transition temperature of the system as a function of cure time, respectively. These events serve as convenient

boundaries that divide the network building process into three distinct phases, each with a distinct mode of network growth.

Prior to gelation, network growth is characterized by the reaction of individual monomer species and the consequent formation of isolated domains of reacted material. The system is a liquid that is completely soluble in an appropriate solvent during this stage of the reaction. The reaction is under chemical control as there is no molecular network present to restrict diffusion. The viscosity of the system increases dramatically during this phase of the reaction due to the incipient formation of larger and larger mass molecular fragments. The mass of the isolated domains of reacted species increases until they link together to form a network whose size takes on the dimensions of the entire sample. This point marks the initial appearance of an infinite molecular weight network and the system gels. This is the end of the pre-gelation stage of network growth and the beginning of the main stage of network growth.

The main stage of network growth is characterized by the addition of mass to this sample-wide molecular network. The sample-wide network is an insoluble gel fraction surrounded by a soluble fraction that consists of lower molecular weight species and unreacted monomer. The mass of the network increases at the expense of the soluble fraction throughout this stage of the reaction. The crosslinked molecular network is sparse enough during the initial part of the main stage of network growth that, for the most part, unreacted species are still able to diffuse freely to active reaction sites and the system remains under chemical control. At first, the sparsely crosslinked molecular network restricts diffusion of only the largest molecular fragments to active reaction sites. As the reaction proceeds and the crosslink density of the system increases, however, the

diffusion of smaller fragments also begins to become restricted until even unreacted monomer is unable to diffuse through the network to add mass at active reaction sites. At this point the sample is said to have undergone vitrification and the sample is entirely under diffusion control.

The final stage of network growth, post-vitrification, marks the effective end of network development. At vitrification the system transforms from a rubbery to a glassy solid. The sample vitrifies as the glass transition temperature of the thermoset material approaches the reaction temperature. Vitrification decreases the molecular and segmental mobilities to such an extent that the chemical reaction is essentially quenched. Unreacted species are no longer able to diffuse to active reaction sites. Further reaction is still possible however, provided the sample did not reach full conversion prior to vitrification.[50] Heating beyond the glass transition temperature is required to appreciably drive further conversion.

General descriptions of the molecular connectivity and mode of network growth can now be given for each stage of the network building reaction. During the pre-gelation phase no network is present and the system consists of finite molecular weight oligomers suspended in a sea of unreacted species. An infinite molecular weight network first appears at the start of the main stage of network growth. The main stage is characterized by the presence of a highly plasticized "skeleton network" to which mass is added throughout the course of this stage of network development. This stage is marked by the shift of the network building reaction from chemical to diffusion control. The last stage of network growth, the post-vitrification stage, marks the effective end of network growth as unreacted species are no longer able to diffuse to active reaction sites.

These descriptions of the state of the network provide a good rough description of the general connectivity within the developing network at a given time of the network building reaction. Through the use of a time-temperature transformation diagram, it is simple to obtain samples with the desired level of connectivity simply by stopping the curing reaction after the appropriate amount of cure time.

Models of Network Formation

Thermosetting epoxies, like all thermosetting polymers, must reach a point during the polymerization reaction where some fraction of the previously isolated monomer and low molecular weight oligomer units has become large enough to form a connected structure with dimensions on the size of the reaction container. Step growth reactions do not form high mass polymers until the late stages of the reaction, meaning that prior to gelation there is a sort of induction period where the major network building reaction consists mostly of reactions between monomer and low molecular weight oligomer.[51] The present work will show that the sub-100 nm morphology, and consequently the homogeneity of the molecular network, is dictated by the manner in which these oligomers develop prior to the formation of the sample-wide network. This step-growth reaction during the initial stages of network formation, like most reactions, can be controlled to some degree by the reaction conditions, especially the reaction temperature. For the resin system studied here, this opportunity is afforded by the temperature dependence of the reactivity ratio between the primary and secondary amine which allows a degree of control over the relative rate of production of linear versus crosslinked segments. To begin, however, the nature of gelation in thermosetting polymers will first

be discussed. This section presents an overview of a few selected classical models of crosslinked network formation.

Statistical Models of Gelation

Any consideration of the nature of the gelation of polymeric materials must first begin with a discussion of the fundamental studies conducted by Carothers over 70 years ago with later refinement by Flory and Stockmayer.[52-54] These studies, at the most basic level, are calculations of the level of conversion required to drive the degree of polymerization to infinity. Flory noted that "since gelation occurs only when there is the possibility of unlimited growth in three dimensions, the conclusion that it is the result of the formation of infinitely large molecules has been irresistible."[53] Flory is quick to point out, however, that this does not mean that the entire crosslinked system *necessarily* consists of a single, macroscopic molecule with an infinite molecular weight, rather, the system may in fact consist of a small fraction of "infinite" molecules while the remaining material reacts only to form relatively small molecules. Two statistical treatments of the increase in the degree of polymerization have been used to describe the gelation of polymers: The statistical divergence of the number average degree of polymerization to infinity developed by Carothers and the statistical divergence of the weight average degree of polymerization to infinity developed by Flory and Stockmayer.

The Carothers equation is one of the simplest descriptions of the relationship between monomer conversion and gelation of a polymer system.[52] This equation relates the gel point of the system to the average functionality of the system when the two reactive groups are present in equal amounts.[55]

The first step is the calculation of the average functionality of the molecules which make up the resin system. The average functionality is simply the number of functional groups per molecule averaged over all types of monomer molecules in the system. The average functionality of the system is therefore simply given by:

$$f_{avg} = \frac{\sum N_i f_i}{\sum N_i} \tag{9}$$

where N_i is the number of molecules of a given monomer and f_i is the functionality of that monomer. These terms are summed over all of the monomer species present in the system.

For the case of the difunctional Epon 828 cured with a tetrafunctional 3.3'-diaminodiphenyl sulfone system mixed in a 1:1 ratio by functional groups, the average functionality is then given by:

$$f_{avg} = \frac{0.26mol_{828}\times 2 + 0.13mol_{DDS}\times 4}{0.26mol_{828} + 0.13mol_{DDS}} = 2.66 \tag{10}$$

(It is important to note that Epon 828 is not simply DGEBA, rather it is a mixture of DGEBA with a small amount of higher molecular weight species as shown in Figure 2. This distribution of molecular weights must be accounted for in the calculation.)

Carothers then related the value of f_{avg} to the conversion at the gel point as follows: First, the extent of reaction in terms of the functional groups lost can be described by:

$$p = \frac{2(N_0 - N)}{N_0 f_{avg}} \tag{11}$$

where N_0 is the number of total monomer molecules initially present, N is the number of molecules after some reaction has occurred while the total number of functional groups is given by $N_0 f_{avg}$. Next, the number average degree of polymerization is given by the

initial number of monomer molecules present divided by the number of monomer molecules present after reaction has been allowed to occur for some time:

$$\overline{X}_n = \frac{N_0}{N} \tag{12}$$

Equations11 and 12 can be combined and rearranged to relate the conversion of the system, p, to the number average degree of polymerization, $\overline{X}_n$:

$$p = \frac{2}{f_{avg}} - \frac{2}{\overline{X}_n f_{avg}}$$

When the number average degree of polymerization diverges to infinity this equation becomes:

$$p_c = \frac{2}{f_{avg}} \tag{13}$$

For the case of the Epon 828/3,3'-diaminodiphenul sulfone system studied here:

$$p_c = \frac{2}{2.66} = 0.75 \tag{14}$$

Carothers' treatment, therefore, predicts that the Epon 828/3,3'-diaminodiphenyl sulfone system should gel once the extent of the reaction reaches 0.75.

Flory and Stockmayer used a statistical analysis of network formation to develop a model to predict when a crosslinking system will reach the gel point by calculating the conversion at which the weight average degree of polymerization will diverge to infinity. This analysis is based upon the determination of the *branching coefficient*, which is the probability that a branch unit can trace a path through a chain segment to reach another branch unit. For a system to be considered gelled, there must be at least one macromolecule within the sample where at least one functional group on all of the branch units within the molecule is connected to another branch unit through a chain segment. This analysis shows that, for the case of the Epon 828/3,3'-diaminodiphenyl sulfone

system mixed in a 1:1 stoichiometric ratio by reactive groups, the extent of the reaction at the gel point can be given by:[51]

$$p_c = \frac{1}{[1+(f-2)]^{1/2}} \tag{15}$$

where p_c is the critical conversion for gelation and f is the functionality of the branch unit (for the present work $f = 4$). The critical conversion at the gelpoint for the present system, therefore, is:

$$p_c = \frac{1}{[1+(4-2)]^{1/2}} = 0.58 \tag{16}$$

The system is predicted to gel once the extent of reaction reaches 0.58.

These models of gelation have their shortcomings. First, the statistical analysis is premised on the idea that the functional groups of the monomer units show identical reactivities. As discussed previously, this is not true for aromatic amine-cured epoxies. Additionally, these treatments ignore the possibility of intramolecular reaction. Flory recognized these deficiencies and noted that these types of statistical treatments are best used as a guide for estimating the development of thermosetting polymers. Regardless of these deficiencies, these statistical treatments serve as an excellent starting point for developing an understanding of general network formation in thermosetting epoxy-amine polymers. As these analyses ignore the influence of unequal reactivity ratios and intramolecular crosslinking, the conversion at gelation predicted by these models can be compared to empirical results in order to gauge the influence of these processes on the development of the epoxy-amine network.

Labana, et al., examined the influence of intramolecular crosslinking on the development of structure within the molecular network and developed a statistical theory that demonstrates the influence of configurational restrictions on the growing network.[56]

The authors noted that after partial crosslinking the network chains are no longer able to assume all previously possible conformations. As an example, the authors described the formation of a large ring with entrapped unreacted species. These entrapped species would then be more likely to react locally within the ring thereby leading to a localized region of relatively higher crosslink density. In their analysis, the authors noted that, to a first approximation, the growing network chains behave as flexible, randomly coiling, freely jointed chains. If the system initially takes on a linear structure (as would be expected if the primary amine is initially consumed faster than secondary amine), then the monomer units of this linear molecule will be distributed around the center of gravity in a Gaussian distribution, as shown by Bueche and Debye.[57] Using the distribution analysis of Bueche and Debye, as well as details of the mean square radius of gyration developed by Zimm and Stockmayer[58], the authors went on to examine the influence of the appearance of crosslinks on the distribution function a model polymer. The authors point out that, even if the initial reactions are intermolecular branching reactions, the segment density at the center of gravity remains very similar to that of the original molecule. The effect of this is that intermolecular reactions do not significantly influence the subsequent likelihood of an intramolecular reaction throughout the branching process. When an *intra*molecular crosslink occurs, however, the internal crosslink severely restricts the number of possible conformations the chain is able to assume and the segment density near the center of gravity increases, increasing the possibility of further intramolecular crosslinking reactions near the center of gravity. The authors point out that this behavior favors the formation of what they term "gel balls" within the architecture of the crosslinked molecular network as the excessive intramolecular

reactions reduce the amount of material available for the formation of intermolecular connections. This behavior will lead to regions of relatively higher crosslink density surrounded by an interstitial region of relatively lower crosslink density. It is the opinion of this author that this is the major driving mechanism for the observed nodular morphology common to cured epoxy-amine systems.

The Influence of Network Architecture on Macroscopic Properties

So far, much has been said about development of structure within the crosslinked molecular network. This section will introduce a few selected studies that illustrate *why* the structure of the crosslinked network matters. The studies overviewed here illustrate the scaling of structure/property relationships from the submicroscopic to the macroscopic scale. Just as these examples show that global differences in the network structure influence bulk physical properties, it is reasonable to expect that localized differences in network structure will lead to regions with different physical properties.

Many research studies have focused on the permeation of solvent, especially water, in epoxy networks. This interest is understandable, as the presence of small molecules within the molecular network can act as a plasticizer and therefore degrade performance while also increasing the mass of the finished part. A study by Douglas, et al. investigated water permeation in an epoxy system with a liquid crystalline structure versus a similar system with a non-liquid crystalline structure. [59] The authors recognized the importance of what was described as the "dual-phase" structure of cured epoxy-amine systems in the ability for water to permeate into the crosslinked network. In fact, an AFM image of the non-liquid crystalline system was shown that exhibited the nodular substructures that are the focus of this work. A corresponding AFM image of the liquid

crystalline system was not shown and it was unclear if the liquid crystalline system possessed a similar morphology. The liquid crystalline sample showed a lower permeability and diffusion coefficient. This behavior was attributed to the smectic phase of the liquid crystalline sample serving as a barrier to penetration of water molecules by reducing the accessible free volume. It was also found that off-stoichiometric samples of the non-liquid crystalline polymer showed the highest permeability to water, with amine-rich samples displaying a greater permeability than epoxy rich samples. This behavior was attributed to the exacerbation of the typical two-phase morphology consisting of higher and lower crosslink density regions due to higher amounts of unreacted material in the off-stoichiometric system. It was pointed out that water is likely to prefer the lower-crosslink density regions due to the higher amount of accessible free volume and this effect is greater due to the higher potential for hydrogen bonding in the amine rich system. Stoichiometric samples showed the lowest permeability and this behavior was attributed to the formation of a greater number of highly crosslinked regions that presented a barrier to water transport. This work shows that the differences in the distribution of crosslinks plays a role in water permeation.

Recent work by Jackson, et al. investigated the influence of free volume hole-size on fluid ingress in epoxy systems.[9] A variety of epoxy monomers were reacted with 3,3'-diaminodiphenyl sulfone and 4,4'-diaminodiphenyl sulfone to yield a series of molecular networks with similar chemical environments, but different average free volume hole sizes as measured by positron annihilation lifetime spectroscopy (PALS). These networks were then exposed to water and other solvents to determine the influence of network architecture on solvent uptake. PALS interrogation showed that epoxy-amine

systems cured with 3,3'-diaminodiphenyl sulfone showed a lower average hole free volume size and this was attributed to a higher order of packing available to the meta-substituted isomer due to higher conformational freedom of the molecular segment over the para-substituted 4,4'-diaminodiphenyl sulfone. 4,4'-diaminodiphenyl sulfone showed higher moisture uptake than 3,3'-diaminodiphenyl sulfone. This behavior was attributed to the ability for water molecules to follow free volume pathways through the network. Subsequent DMA testing showed the presence of two broad peaks in the tan δ of an epoxy system cured with 4,4'-diaminodphenyl sulfone. This behavior was attributed to increased apparent heterogeneity as water disrupted secondary bonds between the hydroxyl and tertiary amine moieties. It was noted that this disruption of intermolecular bonding allowed heterogeneities in the molecular network to become apparent in the form of the dual, broad tan δ peaks. This work noted the likely heterogeneity of the crosslinked molecular network.

Levita, et al., conducted a study on the influence of crosslink density on the fracture toughness of a series of epoxy resins cured with aromatic amine curing agents chosen to yield networks with a variety of crosslink densities.[60] The fracture resistance was found to decrease with increasing crosslink density. This behavior was attributed to a decrease in the number of conformational states available to the polymer which restricts the ability of the material to deform plastically at the crack tip, thereby reducing the amount of propagation energy that can dissipated within the region of the propagating crack tip.

Escher studied the influence of crosslink density on the coefficient of thermal expansion of a series of epoxies with similar chemical structure but different molecular

weights.[61] All experiments were conducted far below the glass transition temperature (down to around 10 K). The coefficient of thermal expansion was found to increase with increasing molecular weight between crosslinks. At higher temperatures (above 150 K), an increase in the coefficient of thermal expansion with increasing molecular weight between crosslinks was attributed to the larger number of methyl groups present on the chain available to begin molecular rotation. The temperatures studied in this work were too low to observe crankshaft and other rotations in the polymer backbone that would be expected to influence the coefficient of thermal expansion at temperatures closer to normal use temperatures.

These studies of the scaling behavior from the molecular scale to the bulk scale are usually based upon the assumption of a continuous three-dimensional network. There is, however, a significant amount of evidence presented in the literature that this is not the case for cured epoxy-amine networks, to the detriment of efforts to develop scaling relationships. The next chapter presents an overview of non-homogeneity in the crosslinked epoxy-amine system in order to underscore the need for a better understanding of the architecture of the crosslinked molecular network at the mesoscale.

CHAPTER III

NON-HOMOGENEITY IN THE EPOXY-AMINE NETWORK

Chapter Overview

Epoxy-amine networks have long been suspected of possessing a non-homogeneous distribution of crosslinks within the network structure. A characteristic nodular morphology has been reported as indicative of the heterogeneous nature of cured epoxy-amine networks. This morphology has been observed under a variety of cure conditions and is found at both the fracture surface and at surfaces etched by ion and ultra-violet radiation, indicating that the nodular nanostructures are a real component of the network and do not result from either a fault in processing or from the fracture process. This chapter presents a review of available literature regarding the detection of non-homogeneous structure as well as a discussion of the likely structure of the crosslinked molecular network. Additionally, efforts to control the observed morphology of the system are reviewed.

Evidence of Non-Homogeneity in Thermoset Networks

Errath and Spur conducted one of the first Western investigations into the substructure of thermosetting polymers.[62] A scanning electron microscope was used to observe a distinct nanoscale morphology in thermosetting resins. A series of thermosets including phenolic, diallyl phthalate and epoxy resins were cured and the resulting morphology was characterized. “Globular” structures or “micelles” were noted with dimensions of 40-90 nm. The development of these structures was attributed to localized regions of rapid polymerization during the network building process. The presence of

these structures was cited as a possible reason for discrepancies between theoretical and observed tensile strengths of these materials.

In another study, Racich and Koutsky used scanning electron microscopy to examine the free surface, fracture surface and solvent etched surfaces of a variety of commercially available epoxy systems.[63] The morphological characteristics of regions cured in the vicinity of glass, silicone rubber, PTFE and copper surfaces were also investigated. The characteristic nodular structure was distinctly observed at all surfaces, but was the most clear on etched surfaces. The nodules were reported to range in size from 10-60 nm in size with samples cured near the silicone rubber having the smallest size and samples cured near the copper substrate the largest size. The authors found this result surprising, and noted that the reason for this was not entirely clear. Plasticization of the network by contamination on the surface of the copper was put forth as a possible reason for the discrepancy in sizes. The possibility that this morphological difference was a result of shrinkage-induced stresses due to different coefficients of thermal expansion of the substrates was also considered. It was noted that clusters of nodules appeared to form together into "supernodules" in some instances. Additionally, the free surface of samples was found to appear smooth, but chemical etching of these surfaces revealed nodular structures typical of bulk structure just below the surface.

Mijovic and Koutsky obtained SEM images of the fracture surfaces of a variety of epoxy systems.[64] Nodules ranging in size from 10-45 nm were reported. The authors noted that fracture tended to propagate around the nodules, indicating that these structures consist of a more highly crosslinked region. It was noted that the basic nodular morphology was not found to be affected by various postcure treatments. The authors

pointed out that this indicates that the nodules probably form prior to gelation. (The present work, however, shows that the nodular morphology appears after gelation, but prior to the onset of vitrification). The authors reported the presence of the nodular morphology in all regions of the fracture surface. Similar results were obtained in the present work. The fact that this nodular morphology is found both in regions where the crack tip propagates elastically as well as in regions where plastic flow was observed at the macroscopic scale provides strong evidence that the observed morphology is a consequence of the underlying network structure rather than an artifact of the fracture process. Further analysis showed that nodules located in regions that underwent plastic deformation during the fracture process appeared to be "carried" intact along with the surrounding matrix during the flow process, providing reason to believe that the nodular structures are regions of higher crosslink density surrounded by an interstitial region of lower crosslink density capable of flow. In a separate study, Morgan and O'Neal subjected an epoxy amine system to strain while being monitored in a scanning electron microscope.[65] Six to nine nanometer structures were observed and these structures remained intact even as the surrounding material flowed in response to the strain.

More recently, atomic force microscopy has been used to characterize the nanoscale morphology of epoxy-amine samples. Gu, et al. used AFM in an investigation of the influence of outdoor exposure on an epoxy-amine coating.[66] Samples were obtained of a free surface, a surface cured at the interface of a silicone mold and bulk material was also obtained by microtoming a sample. The commonly observed nodular morphology was observed in both the sample cured at the interface of the silicone mold as well as bulk material. The sample cured at the free ambient surface, however, was

found to be smooth (similar behavior was observed in the present work). It was explained that the smoothness of the free surface sample may be a result of low surface-energy contaminants migrating to the surface during the low viscosity stages of network development and this contaminant layer obscures the underlying nodular structure. As part of their investigation into the effects of outdoor exposure, the authors exposed this smooth surface to outdoor conditions for 70 days and then re-imaged the surfaces. Severe degradation of the previously smooth surface was observed in the form of pits or craters where the topmost layer was no longer present. These pits were approximately 20 nm deep and the distinct nodular morphology could clearly be seen within these pits, indicating that the nodular morphology was lying just beneath the topmost smooth layer. The authors also showed AFM phase images of the samples which showed clear regions with different tip/sample interaction. The distribution of these areas matched the position of the nodular structures seen in the topographic images. The authors attributed this phase contrast to the tip interacting with a stiffer, higher crosslinked region at the core of the nodule and a less stiff, lower crosslinked region in the interstitial region, however, no consideration was given to the possibility that the observed phase shift was a result of the sharp change in surface slope at the boundary of individual nodules.

Other characterization techniques have also indicated a non-homogeneous structure in epoxy-amine networks. Matyi, et al. characterized the structure of an epoxy-amine system with small-angle X-ray scattering.[67] The authors reported that heterogeneity on the order of 25 nm or larger would be required to explain the observed scattering behavior of the samples. It was noted that this heterogeneity could be caused by "supermolecular arrays of regions which differ in crosslink density" or, alternatively,

dirt or air bubbles may be responsible. The author notes that non-homogeneity at smaller (less than 10 nm) and much larger (above 400 nm) was also detected, although in lesser amounts. The authors acknowledged that the dimensions of the detected non-homogeneity were at the correct scale to correspond to the presence of the commonly observed nodules, however, they were hesitant to make the connection between regions with different scattering intensity and the nodular morphology.

Mijovic and Tsay examined the dynamic mechanical behavior of an epoxy-amine system in light of potential non-homogeneity in the architecture of the crosslinked network.[68] The authors stated that samples cured with higher amounts of curing agent should lead to networks with higher internodular crosslinking at the expense of intranodular crosslinking, although the reasoning behind this claim was not entirely clear. Therefore, the authors stated they could produce samples with variable relative amounts of internodular crosslinking and intranodular crosslinking. Systematic dynamic mechanical analysis of a variety of formulations showed that the storage modulus of the sample was primarily determined by the less-crosslinked internodular material while the glass transition temperature of the network was dependent upon the crosslink density within the nodules.

Gu, et al. used small angle neutron scattering to investigate the structure of the molecular network architecture of an epoxy-amine coating.[69] Cured samples were soaked in deuterated acetone to enhance neutron contrast. A well-ordered structure was found at the scale of around 50 nm. This size scale corresponded to the size of nodules observed via AFM in the same study. This structure was reported to be a result of the deuterated acetone preferentially swelling the low-crosslink density interstitial region. This type of

preferential swelling behavior supports the theory that this lower crosslink density interstitial region presents a low-energy propagation pathway for the influx of small molecules into the network.

These studies were conducted on a wide variety of amine-cured epoxy systems cured under diverse conditions. Each study reported the observation of a similar nodular morphology with structures that range from 10 nm to around 80 nm. Multiple researchers have proposed that these nodular structures are composed of regions of relatively higher crosslinking surrounded by an interstitial phase of relatively lower crosslink density and that opinion is shared by this author.[56, 59, 64, 65, 70, 71]

Initial AFM studies conducted as part of the present work showed that the sub-100 nm morphology of samples of various composition, filler content and processing history are very similar. Figure 6 shows representative AFM images of the fracture surface of cured epoxy-amine samples obtained during the initial stages of the present work. Figure 6a shows AFM topographic (left) and phase images of an Epon 828/3,3'-diaminodiphenyl sulfone network. Figure 6b shows AFM images of an aerospace-grade carbon fiber reinforced epoxy-amine system that had been cured in an autoclave according to the manufacturer-specified cure schedule. This image was obtained from a section that had previously been protected by a layer of peel-ply. Removal of the peel-ply also removes the topmost layer of the composite surface, producing a fracture surface (the carbon fibers are below this topmost surface and cannot be seen in this image). Figure 6c shows AFM images of a DGEBA epoxy resin cured with 4,4'-diaminodiphenyl sulfone that had been modified with a proprietary thermoplastic modifier. The

characteristic nodular morphology is observed in each system indicating that these substructures are common to epoxy-amine thermoset polymers.

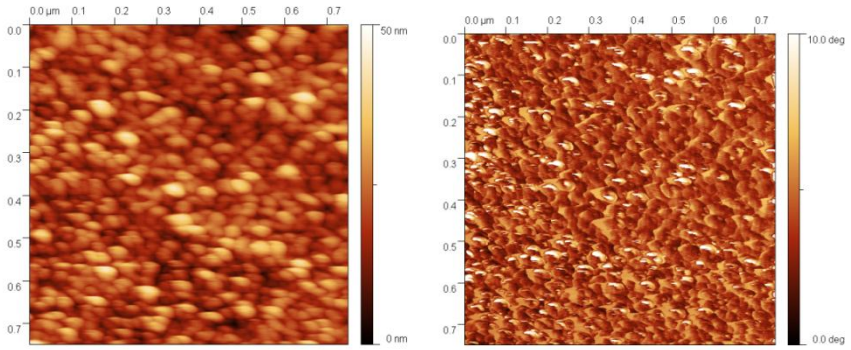

(a)

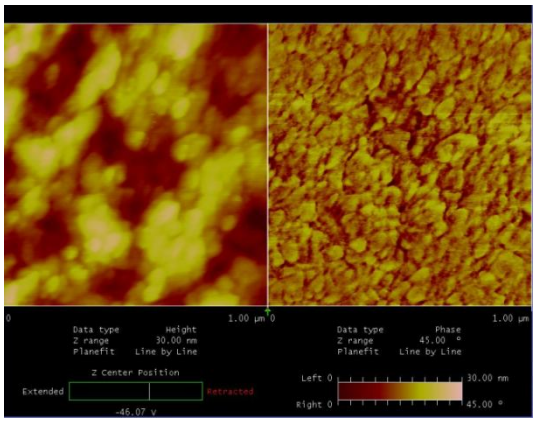

(b)

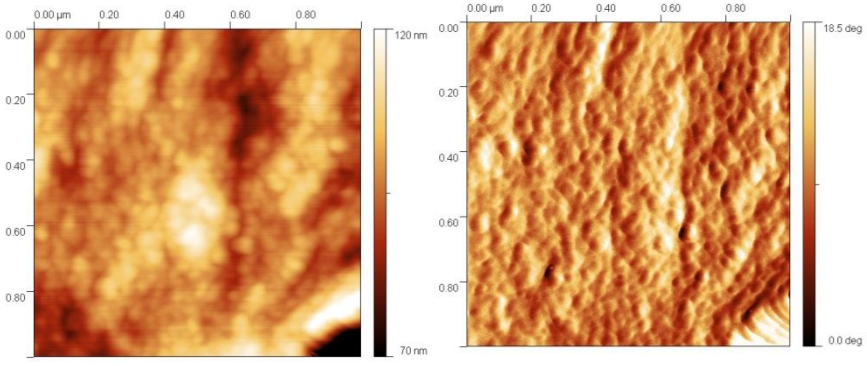

(c)

Figure 6. AFM topographic (left) and phase images of a variety of epoxy-amine networks. The distinct, nodular morphology can be observed in each sample despite differences in chemical composition and processing history. Lateral dimensions: (a) - 750 nm; (b) - 1000 nm; (c) - 1000 nm

The Debate of Homogeneity versus Non-homogeneity

The claim that the observed nodular morphology was indicative of non-homogeneity in the crosslinked molecular network sparked an active debate regarding the inherent heterogeneity of the epoxy-amine network architecture. Now, most studies reported in the literature seem to agree that epoxy systems likely possess a non-homogeneous molecular network structure. The following section, however, will give a brief overview of the major studies that question the claim of a heterogeneous epoxy-amine network.

Dusek, et al. questioned the inherent heterogeneity of the cured epoxy-amine network.[72, 73] The authors question the use of electron microscopy to detect the nodular structure. This technique was criticized due to the potential for the electron beam to interact with the sample in such a way that the commonly observed nodular morphology is, in fact, etched onto the surface during imaging. While this is a valid point, interrogation by atomic force microscopy is free from this type of etching artifact yet samples still show the distinct nodular morphology.

Additionally, the authors noted that micrographs of linear amorphous samples also possessed a nodular structure. This was cited as evidence that the observed substructure was not necessarily due to the crosslinked network. The present work, however, did not find this to be true. Figure 7 shows AFM topography images of two different polymer samples. Figure 7a shows the fracture surface of the crosslinked epoxy studied in this work while Figure 7b shows the fracture surface of a commercially available polystyrene. Nodular substructure is clearly seen in the crosslinked polymer while the linear polymer shows a much smoother morphology.

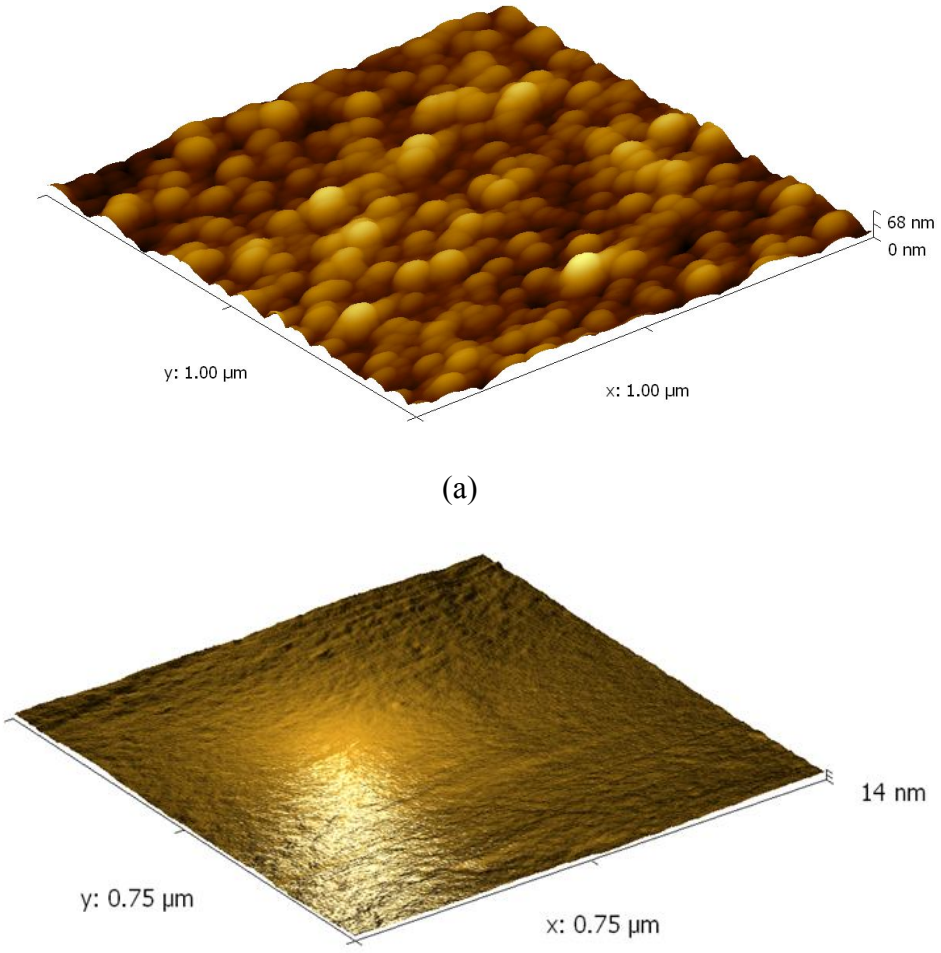

Figure 7. Three dimensional projection of AFM topographic data of the fracture surface of a crosslinked epoxy (a) and a thermoplastic polystyrene (b). The distinct nodular morphology is clearly seen in the crosslinked material but not in the linear material.

Dusek goes on to cite the lack of evidence of heterogeneity in small angle x-ray scattering studies even after swelling with a solvent of different electron density as an indication of the homogeneity of epoxy-amine networks. This is counter to the results reported by Gu.[66, 69] Overall, the authors do not seem to deny the possibility that non-homogeneity in the network may develop, rather, an argument is made that non-

homogeneity is not a necessary condition of cured epoxy-amine networks. The authors point out that "thermodynamic instability" resulting from the crosslinking process or localized regions of higher concentration of the curing agent may induce non-homogeneity in the crosslinked network.

Controlling Morphology

The ability to control the crosslinked molecular network architecture in epoxy-amine networks is desirous as it is expected to enable a degree of control over bulk properties from the molecular scale. To this end, multiple studies have been conducted to correlate changes in the topology of the molecular network to bulk scale properties.[12, 74-76] However, these studies tend to have an implied assumption of an overall homogeneous network structure. Other work has been conducted in an attempt to correlate chemical structure or processing characteristics to the commonly observed nodular morphology, however, as will be shown, these attempts are not as successful as one would hope.

Mijovic and Koutsky studied the influence of different postcure regimens on the nodular morphology of system similar to the one studied in the present work.[77] As with the previously described studies, the characteristic nodular morphology was observed in SEM images on all fracture surfaces. Neither the size nor the shape of the nodules were observed to be dependent upon either the postcuring time or the post curing temperature. It was not possible to deduce if the act of postcuring itself, however, induced a change, as no images of non-postcured samples were presented for comparison. However, the present work indeed shows a post-curing induced change in the sub 100-nm morphology.

Bell attempted to reconcile the extent of monomer mixing on the development of nodular morphology of a cured epoxy amine system similar to the one used in the present

work.[78] Bell used an automated shear mixer that was reported to produce highly repeatable levels of mixing. The typical nodular morphology was observed with transmission electron microscopy and it was noted that less vigorous mixing produced larger nodules while very vigorous mixing produced samples with little evidence of the nodular nanostructure. Subsequent tensile testing showed that samples with larger nodules showed lower tensile strengths than samples with less evidence of a nodular substructure, although the differences were not especially dramatic.

Vanlandingham, et al. studied the relationship between stoichiometry and substructure in an epoxy-amine system similar to the one studied in the present work.[79] Stoichiometric and off stoichiometric samples were prepared and the resulting morphology was interrogated with atomic force microscopy. The nodular morphology was observed in all samples. Samples with higher concentration of epoxy were observed to yield smaller nodular domains. Samples cured with a higher concentration of amine were reported to have a larger distribution of nodule size.

Overview of Heterogeneity in the Epoxy-Amine Network

The present work adds to the discussion of heterogeneity in the cured epoxy-amine network by examining the growth of the nodular substructure. A clear ability to influence the manner of nodule growth by adjusting the processing temperature was found. The nodular nanostructures are especially clear at the fracture surface of samples and, as shown by this work, appear only after the gel point and become more distinct as cure progresses. This behavior indicates that these structures result from the underlying molecular network and that their presence influences the crack tip propagation pathway.

CHAPTER IV

FRACTURE PATHWAY AS AN INDICATOR OF UNDERLYING NETWORK STRUCTURE

The previous chapter provided an overview of the likely heterogeneous nature of epoxy-amine molecular networks. These heterogeneous regions, for the most part, have been reported to have a characteristic dimension of around 40-60 nm and, as will be seen, this is also the scale of the substructure investigated in this work. In order to characterize their nature, there must be a physical way to probe the material at this scale. As discussed previously, traditional molecular (or even sub-molecular) scale techniques such as NMR, NIR and PALS provide valuable information about monomer connectivity and the amount of free-volume within the network, however, they lack the ability to resolve lateral distance. These techniques are unable to provide information about the *distribution* of connectivity within the molecular network. Similarly, thermal and mechanical techniques provide information about the influence of connectivity within the network, however this information tends to be "averaged" over the connectivity of the bulk network, again, with the lack of lateral resolution.

Even AFM, whose normal operation lies comfortably at the mesoscale, lacks the ability to *truly* interrogate the structure of a sample. To obtain information about the state of the network, some type of information must be input into the network, usually in the form of energy. For example, NIR spectroscopy introduces infrared radiation into a sample, NMR spectroscopy introduces RF magnetic fields into a sample and rheometry introduces force into a sample. These techniques are then able to provide information about the sample by measuring how the sample alters the input energy. Since AFM is a

microscopic technique, the act of simply obtaining topographic AFM images of a sample does not characterize the structure of a material. Rather, in the strictest description of what is actually occurring, the AFM is simply providing an image of the state of the morphology at the mesoscale.[a] A mesoscale "probe" is required to provide information about the structure of the network. In what is believed to be a unique solution to this dilemma, the present work uses a propagating crack tip as this mesoscale probe to cause a response in the network, and then uses AFM imaging to measure how the sample responded to this energy input, therefore allowing information about the underlying structure of the molecular network to be obtained. As described in the introduction, the propagation pathway is expected to deviate in response to the structure of the network so that the propagating crack tip follows the lowest energy propagation pathway, therefore preserving it at the surface for later AFM interrogation.

One of the basic tenants of continuum fracture mechanics is that material strength is governed by the presence of flaws.[80-82] The presence of flaws is used to explain the fact that material strengths tend to be much lower than theoretical strengths. It is reasonable to anticipate that regions of non-homogeneous distribution of crosslinks contribute flaws to the structure of the network. Fracture mechanics is mostly concerned with bulk behavior of materials. Consequently, most concepts of fracture mechanics are premised upon the assumption of a continuously homogenous three dimensional network.[81, 83] The effect of this underlying assumption is that these concepts may not find appropriate application for analysis of material behavior at the dimensions studied as

[a] This statement is not the case for AFM phase imaging; however, due to the inability to deconvolute variation in tip/sample interaction caused by network structure from variation in tip/sample interaction caused by sharp changes in slope with absolute certainty, phase imaging was not used to deduce information about network structure in this work.

part of this work (that is, continuum fracture mechanics relationships are inappropriate at this scale because the material does not have continuous properties) . For example, calculations on the amount of energy lost to plastic deformation are typically based on a deformation zone that is either spherical or ovoid in shape with homogenous material properties within this zone.[83, 84] This assumption of homogeneous material properties will not be appropriate if the zone of plastic deformation is larger than the characteristic dimension of the observed nodular non-homogeneities. Regardless, plastic deformation undeniably contributes to the energy required to fracture an epoxy-amine network.[25, 81, 83] A question more pertinent to the conclusions of this work, however, is the question of the contribution of plastic deformation to the resulting morphology of the fracture surface. All samples studied in this work, even samples that had not yet reached the gel point, were well below their glass transition temperature to ensure that they were in a glassy solid state with little expected ability to flow within a reasonable time scale. This resistance to flow-induced deformation was demonstrated even at the nanoscale through nanoindentation studies. The results of this will be presented in a subsequent section, for now, however, it is sufficient to say that severe plastic deformation was not observed in the samples studied in this work.

Other studies have confirmed that plastic deformation does not appreciably influence the resulting fracture surface morphology of epoxy-amine systems. The previously mentioned study by Mijovic and Koutsky noted that material appeared to have undergone flow at the scale of a few nanometers during the sample process, as evidenced by the apparent alignment of nodular structures in what can reasonably be identified as a flow pattern.[64] The nodular substructures in the flow region are identical to those that did

not experience flow indicating that plastic deformation during the fracture process does not disrupt the structure of the nodules. In another study, Morgan and O'Neal strained an epoxy-amine system while observing the material response with a scanning electron microscope.[65] The authors reported the observation of six to nine nanometer sized particles that remained intact even as the flow process was occurring. The authors noted that those regions of lower crosslink density surrounding these structures appeared to undergo plastic deformation while the observed structures resisted it.

Fracture Pathway as an Indication of Underlying Network Structure

This work borrows the concept of the "critical manifold" from the field of grain boundary engineering of metals and ceramics in order to describe the fracture behavior of the epoxy-amine system. The concept dictates that, in much the same way that a propagating crack tip will preferentially travel along the weakest grain boundaries of a metal, so will a propagating crack tip travel along the regions of lowest covalent bond density in a thermosetting polymer. Holm's work has been instrumental in the development of the use of critical manifolds to understand the relationship between material substructure and fracture propagation pathways.[85-89] This foundational work is primarily based in computational simulations of lowest energy pathways supported with empirical evidence of similar structures found at the fracture surfaces of metals and ceramics. It is anticipated that this type of behavior will hold true for any material that fails under brittle, elastic fracture.

The formation of the critical fracture manifold is an energy-driven process. Consider the Griffith fracture criterion for elastic fracture:[80, 89]

$$E_f = \Delta EA \tag{17}$$

where E_f is the minimum amount of energy required to separate a solid into two pieces, ΔE is the energy required to create some unit of new surface area and A is the new surface area created. The energy expended to create new free surface must be assumed to be minimum, therefore, for the case of a perfectly elastic, perfectly homogeneous sample, the new surface area created is simply the cross sectional area of the sample. For perfectly homogeneous materials the crack tip will traverse the sample in such a way as to produce a perfectly planar fracture surface, thereby minimizing the new free surface area created. (This type of behavior is quite familiar to gem cutters.)

The Griffith fracture criterion shows that, for the case of perfectly homogeneous systems, there is no energy advantage available to induce the propagating crack tip to deviate from planarity as the tip is thermodynamically driven to minimize the amount of new free surface area created. Should the tip encounter a region of non-homogeneity, however, the propagating tip will have a choice to make. The energy required for fracture is always minimized, therefore, the propagating crack tip will choose the lowest-energy path through the system. In the presence of non-homogeneous crosslink density the propagation pathway chosen by the crack tip will be dictated by an energy balance between the energy required to create new free surface and the energy required to break covalent bonds. It is a bit awkward to directly compare the amount of energy required to create new free surface to the energy required to break all bonds within a certain area (especially when considering that bulk surface energy measurements likely do not scale linearly to the nanoscale). Regardless, qualitatively it can be said that to the propagating crack tip, the expenditure of energy on the creation of new free surface energy (around 45 mJ/m^2) is less energetically expensive than the expenditure of energy to cleave through

regions of relatively higher crosslink density (C-C bond strength of 346 kJ/mol). This line of reasoning, of course, ignores many of the other energy contributions and fracture processes that are important to continuum fracture mechanics, however, it is believed by this author that, at the nanoscale, the primary influence on the chosen propagation pathway is determined by the reluctance of the propagating crack tip to expend energy to cleave covalent bonds when it has the opportunity to simply travel around them instead.

In reality, however, the energy balance is much more complicated than the simple choice between breaking carbon-carbon bonds or creating new free surface. Even the interstitial region most likely contains internodular covalent bonds and it certainly contains secondary bonds. The energy balance, then, is mostly likely dominated by the difference between the energy required to cleave individual nodules versus the energy required to cleave a lower number of bonds in the interstitial region. The energies involved in these processes most likely overwhelm the influence of the much lower energy required to create new free surface. The relatively minor difference in internodular and intranodular propagation energy prevents the crack tip from following an absurd path through the material.

Experimentally Observed Critical Manifolds

Deviation in the propagation pathway in response to underlying structure has been reported in thermoplastic systems. This deviation was found to preserve known structural information at the fracture surface. Figure 8 shows two micrographs that demonstrate the propagation pathway of a crack tip through Nylon-6[90] (Figure 8a) and poly(propylene) [91] (Figure 8b).[83] The propagation pathway through Nylon-6 is seen to preferentially travel along lamellar boundaries. These boundary regions are enriched

with chain ends and material that was rejected during lamellar formation and deficient in covalent bonds. Propagation through poly(propylene) is seen to preferentially travel along the boundaries of spherulites. Just as with the lamellar boundaries of Nylon-6, these boundaries are also deficient in strong covalent bonds. These micrographs provide a demonstration of the use of a propagating crack tip as a "probe" of underlying molecular architecture. In a similar way, the present work utilizes nanoscale fracture behavior to identify the distribution of network heterogeneity in a typical epoxy-amine system.

CHAPTER V

EXPERIMENTAL DETAILS

Research Overview

The overall goal of this research is to investigate the development of substructure in an Epon 828/3,3'-diaminodiphenyl sulfone crosslinked network and to develop a method to influence the manner in which it develops. This was accomplished by characterizing the time-temperature transformation behavior of the sample to enable the creation of samples with different states of network development. Near-infrared spectroscopy was then used to determine the molecular structure of the network in order to determine the average crosslinking of the sample. Samples were then fractured, and the critical manifold was interrogated with atomic force microscopy in order to determine the distribution of crosslinks within the molecular network. Special attention was paid to the influence of cure temperature on both the rate of linear versus crosslinked segment production and also the morphology of the critical manifold.

Materials

Diglycidyl ether of bisphenol A (Epon 828) was purchased from E.V. Roberts Co. (Carson, CA). Epon 828 is a low molecular weight difunctional epoxy oligomer that was received as a clear viscous liquid. 3,3'-diaminodiphenyl sulfone (DDS) was purchased from Tokyo Chemical Industry Company. DDS is a tetrafunctional aromatic amine that was received as a fine white powder. The chemical structures of the epoxy component and the amine curing agent are shown in Figure 8. All materials were used as received.

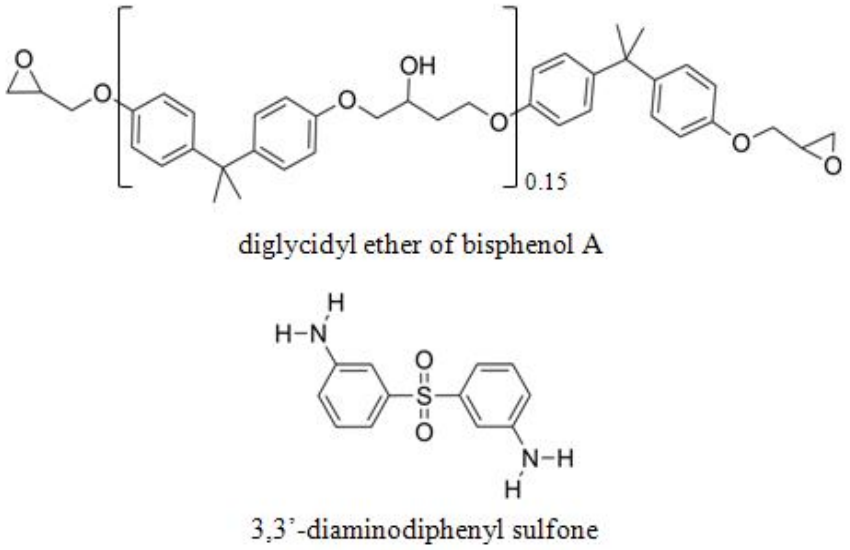

Figure 8. Molecular structure of diglycidyl ether of bisphenol-A and 3,3'-diamino diphenyl sulfone.

Sample Preparation

In order to ensure consistency, all resin was prepared in batches with new resin prepared for each set of experiments. To prepare a batch of resin, one hundred grams of Epon 828 were placed in a standard lab beaker which was immersed in an oil bath heated to 130°C. The Epon 828 was allowed to warm for two minutes then 32.6 grams of DDS were added. These amounts were chosen based on the difunctionality of the Epon 828 and the tetrafunctionality of the DDS in order to yield a 1:1 ratio of the reactive groups. This ensured that, theoretically, 100% of each reactive species would be consumed. The mixture was stirred mechanically at 130°C under normal atmospheric conditions. Each batch was allowed to stir for 20 minutes at which point the mixture was observed to be a clear, low viscosity liquid. The mixed resin was then immediately prepared for specific tests. All samples were subjected to this mixing technique, regardless of the cure temperature used for the final sample preparation. The cure time t=0 is defined to be the

time at which the DDS was added to the Epon 828, therefore, the first 20 minutes of cure time for each sample occurred at 130°C while the sample was stirring.

Determining the Time to Gelation

The time to gelation for each reaction temperature was determined by monitoring the evolution of the dynamic shear moduli during the curing reaction using an ARES Rheometer from TA Instruments (New Castle, DE) equipped with a heating oven that held the sample isothermally at the desired cure temperature for the duration of the test. After mixing, the liquid Epon 828/DDS mixture was poured directly onto 25 mm aluminum parallel plates that had been preheated to the desired cure temperature (between 50°C and 300°C in ten to twenty degree increments). Care was taken to avoid the introduction of air bubbles. Testing was conducted with a gap of 1 mm. The ARES rheometer is capable of MultiWave testing which allows multiple frequencies to be tested simultaneously over two orders of magnitude.[92] This is advantageous as it reduces the amount of time required for measurement. Each test took around 25 seconds, meaning that cure progressed to some degree during the time required to complete the measurement, however, this time is small compared to the overall time the sample was monitored, thus any change in the network from the beginning to the end of each individual test is small enough not to affect the measurement to a large degree. Measurements were made at 0.1% strain as this was likely sufficiently low to avoid non-Newtonian effects and network breakdown. Initial tests were conducted to ensure all measurements were made in the linear viscoelastic region. The storage (G') and loss (G'') moduli were measured every two minutes at frequencies of 0.5 rad/s, 1 rad/s and 50 rad/s simultaneously. These values were used to calculate the loss tangent (tan δ):

$$tan\delta = \frac{G''}{G'} \quad (18)$$

The measured values of the tan δ were plotted as a function of time and the time to gelation was determined by noting the point at which the measured value of tan δ was independent of the measurement frequency.[93, 94] This process was repeated for each reaction temperature as the time to gelation is cure temperature-dependent.

Determining the Time to the Onset of Vitrification

A Q100 differential scanning calorimeter (DSC) from TA Instruments (New Castle, DE) was used to monitor the evolution of the glass transition temperature with cure time. Approximately 12 mg of the mixed resin was placed into hermetically sealed aluminum DSC pans. Samples were held at the desired cure temperature in the DSC for predetermined lengths of time and then thermally scanned from -10°C to 200°C at 20°C per minute. Data was analyzed with TA Universal Analysis v.4.5A. The T_g was taken as the inflection point of the exotherm. The onset of vitrification was accepted as the point where the T_g of the sample no longer increased with additional cure time indicating that the crosslinking reaction had slowed significantly.[48] This point was easily identified by plotting the measured T_g as a function of cure time and noting the time at which the plot showed an obvious change in slope. Due to time constraints, the onset of vitrification was determined rheometrically for samples cured at low temperatures (time to vitrification greater than 500 minutes). This was done by identifying the time at which the storage modulus reached a plateau value.[24]

Determining the Time to the Onset of Degradation

A Q500 TGA from TA Instruments (New Castle, DE) was used to identify the onset of degradation. Approximately 25 mg of uncured resin was placed in a platinum

TGA pan and held isothermally at a desired temperature in air while monitoring any reduction in mass. Data was analyzed with TA Universal Analysis v.4.5A. The onset of degradation was taken to be the point where the sample was observed to have lost 15% of the initial mass.

Determining Monomer Conversion

Monomer conversion was monitored by real-time transmission near-infrared spectroscopy (NIR). After mixing according to the procedure described above, a small amount of resin was sandwiched between two borosilicate glass microscope slides using a 3 mm thick PTFE spacer. A Nicolet 6700 spectrometer from Thermo Scientific (Waltham, MA) equipped with a heating cell was used to monitor changes in absorption in the region from 10,000—4,000 cm^{-1} during isothermal cure at each experimental temperature. Thirty two scans were made during each sampling interval with a resolution of 4 cm^{-1}. Spectral analysis was performed with OMNIC 7.3 analysis software from Thermo Electron Corporation. The concentration of primary, secondary and tertiary amine was determined as a function of cure time from the area of the absorption bands listed in Table 1.

Changes in concentration of each amine species were calculated according to Beer's law following methods developed to discriminate between the concentration of primary, secondary and tertiary amine.[37, 95] The difficulty of preparing samples with identical path lengths was overcome by using the phenyl group band at 4605-4630 cm^{-1} as an internal standard to normalize the integrated peak areas. The absorption coefficients required to calculate concentration according to Beer's law are both frequency-specific and temperature dependent and therefore were calculated for each

chemical species of interest at the frequency ranges listed in Table 1 for each cure temperature. As an example, Table 1shows the calculated values for the sample isothermally cured at 150°C (values calculated for other cure temperatures were similar and are not shown). As volume concentration is difficult to measure in the Epon 828/DDS mixture, the initial molar concentration (expressed as mol kg^{-1}) of each component of interest was used to calculate molar absorptivity. The absorption coefficients of the primary amine and epoxy group were calculated from neat samples of their respective monomer. The molar absorptivity of the secondary amine was calculated by measuring the conversion of primary amine during the first 20 minutes of cure. It was assumed that the only reaction during this time was the conversion of primary amine to secondary amine and no secondary amine was converted to tertiary amine. This assumption is reasonable because of the higher reactivity of a primary aromatic amine compared to a secondary aromatic amine.[29] It should be noted that this assumption is more valid for samples cured at lower temperatures. The concentration of secondary amine at t=20 minutes can then be deduced by measuring the reduction of primary amine concentration during the first 20 minutes of cure. The molar absorptivity of the secondary amine was calculated from its absorbance at 6610-6750 cm^{-1}.

Epoxy concentration at time=*t* was calculated according to the following relationship:

$$[EP]_t = [EP]_0 - [1°Amine]_t - 2[2°Amine]_t \quad (19)$$

where $[EP]_t$ is the concentration of epoxy groups at the measurement time, $[EP]_0$ is the initial concentration of epoxy groups $[1°Amine]_t$ and $[2°Amine]_t$ are the concentration of primary and secondary amine at the measurement time, respectively. It must be noted

that this relationship is based upon the assumption that the etherification reaction of the epoxy groups by hydroxyl groups produced during the reaction makes only a minor contribution to the total epoxy conversion. The reaction of an epoxide with a hydroxyl group is considered to have a higher activation energy than the reaction of an epoxide with an aromatic amine and therefore is less favorable.[33-36] Nevertheless, the possibility of the etherification reaction contributing to the crosslinking reaction to some degree should not be discounted, especially in samples cured at the highest reaction temperatures.

The total absorbance from overlapping bands is the sum of the absorbances of the individual components. The concentration of secondary amine was determined by deconvolution of the absorbance at 6520-6720 cm^{-1} according to the following relationship:

$$A_t = \varepsilon_{1^\circ}[1^\circ\text{Amine}]_t + \varepsilon_{2^\circ}[2^\circ\text{Amine}]_t \quad (20)$$

where A_t is the total band area at time *t*, ε_{1° and ε_{2° are the molar absorptivities of the primary and secondary amines at 6520-6720cm^{-1}, respectively and $[1^\circ\text{Amine}]_t$ is the concentration of primary amine at time *t* calculated from its non-convoluted absorption band at 5040-5100 cm^{-1}.

The tertiary amine concentration was calculated from the balance of primary and secondary amine consumed and produced:

$$[3^\circ\text{Amine}] = [1^\circ\text{Amine}]_0 - [1^\circ\text{Amine}]_t - [2^\circ\text{Amine}]_t \quad (21)$$

where $[3^\circ\text{Amine}]$ is the concentration of tertiary amine at time *t*, $[1^\circ\text{Amine}]_0$ is the initial molar concentration of primary amine and $[1^\circ\text{Amine}]_t$ and $[2^\circ\text{Amine}]_t$ are the concentrations of the primary and secondary amine at time *t*, respectively.

Table 1

Initial molar concentrations, molar absorptivities and wavenumbers of the absorption bands used to quantify NIR spectra for the sample cured at 150°C.

Chemical Group	Absorption Band (cm^{-1})	Molar Absorptivity ($kg\ mol^{-1}$)
Phenyl	4610-4689	5.4
Epoxide	4520-4540	4.4
1° amine	4520-4540	1.3
1° amine	5040-5110	8.7
1° amine	6610-6750	4.9
2° amine	6610-6750	5.0

Fracture Testing

Fracture test specimens were produced by pouring the mixed Epon 828/DDS resin into 75 mm x 15 mm x 7 mm silicone molds. The molds were preheated to the desired temperature before the resin mixture was poured into them and the samples were then isothermally cured up to the onset of vitrification (as determined by prior DSC or rheometric analysis). Some samples were post-cured by holding them at 200°C for an additional 120 minutes.

Fracture testing was conducted according to ASTM D-5045.[96] Low cure temperature samples were extremely brittle and therefore it was not possible to reliably induce a pre-crack. Therefore, it was decided to not pre-crack any of the specimens, despite the protocol called for in ASTM D-5045. For this reason, the fracture test results

reported here are best viewed as a means to compare the fracture toughness of samples within the experimental set fabricated for this work.

The resulting fracture surfaces were saved for imaging via atomic force microscopy.

Atomic Force Microscopy

The fracture surface morphology of the fracture specimens was characterized with a Dimension 3000 atomic force microscope (AFM) from Veeco Instruments (Santa Barbara, CA) equipped with an optical positioning system. Surface topography images were made with a silicon probe with a 125 μm long cantilever and a nominal spring constant of 40 N/m operated in tapping mode at its resonance frequency of around 370 kHz. The tip had a nominal radius of curvature of 8 nm. The cantilever's tapping amplitude during imaging was maintained at around 85%-90% of the free amplitude to minimize cantilever-induced surface deformation while also allowing adequate tracking of the sample surface. AFM imaging was conducted under ambient conditions in a temperature (20°C) and humidity (40-45%) controlled room.

The fracture surfaces that were created during the fracture toughness experiments were cut to size using a high speed diamond saw blade. The cutting process was not found to noticeably contaminate the imaging surface. The samples were then affixed to an AFM stage puck with putty. The fracture surface samples obtained from the fracture testing described above were not macroscopically smooth, as is generally the case for samples interrogated via AFM. The optical positioning system of the AFM provides a magnified image of the sample surface and this magnified image was used to find a suitably flat imaging region. Images were preferentially taken at the "mirror" region of

the fracture surface. However, the mirror region was inaccessible for some samples so images were instead made on the "mist" region of fracture. Initial studies showed that identical nanoscale morphologies are seen on the mirror, mist, and hackle regions of the fracture surface, despite the differences in macroscopic morphology. This provides further evidence that these structures result from the network architecture, not the fracture process.

750 nm x 750 nm areas were scanned at a rate of 0.75 Hz with a resolution of 512 x 512 pixels. Multiple areas were scanned for each sample and figures presented in this document show representative morphology. Images and statistical quantities were processed with Gwyddion v.2.24 SPM analysis software. Image processing was limited to data leveling by plane subtraction and the correction of scan line artifacts. Root mean square (RMS) roughness for each sample was calculated according to ASME B46.1-1995.[97] RMS roughness describes the height deviation of individual data points (pixels) measured from the mean surface-height plane and is given by the following equation:

$$R_{RMS} = \sqrt{\frac{1}{N}\sum_{i=1}^{N} r_i^2} \tag{22}$$

where N is the total number of pixels and r_i is the vertical distance of pixel i from the mean surface-height plane.

Nanoindentation

Nanoindentation-based creep testing was performed with a TI 900 TriboIndenter from Hysitron, Inc. (Minneapolis, MN). Samples were affixed to AFM stage pucks with stiff epoxy putty. A load-controlled loading function consisting of a 100 μN/s loading segment, 60 second hold time at a peak load of 250 μN and a 25 μN/s unloading segment was used for all tests. This force produced an indentation depth on a size scale similar to

that of individual nodules. Three different fracture surfaces of each sample from a specific cure time were investigated. Ten indentations were made on each fracture surface for a total of 30 indentations per cure increment. Creep behavior was determined by monitoring indenter displacement as a function of load hold time. The Oliver-Pharr model was used for data analysis.[98]

CHAPTER VI

THE TIME-TEMPERATURE-TRANSFORMATION BEHAVIOR OF THE EPOXY-AMINE NETWORK

Chapter Overview

In order to elucidate the architecture of a thermoset polymer's molecular network, it is logical to begin by first developing an understanding of the "average" connectivity within the network. The understanding of the average connectivity of the crosslinked molecular network developed in this section is simply a statement of whether or not an infinite molecular weight network is present, and if it is present, whether or not it is still growing. Despite the simplicity of this description of the state of the network, it serves as an important foundation for later refinements of connectivity within the network.

This section develops an initial understanding of network connectivity by identifying the two classic points of network development: the gel point and the onset of vitrification. The identification of these two points is fairly straightforward and can be accomplished through rheological and thermal characterization, respectively. As both the gel point and the onset of vitrification influence the way mass is added to the growing network, these events can serve as convenient boundaries for different modes of network growth. The time to the gel point and the onset of vitrification at a given temperature is highly repeatable. Consequently, knowing the time required to reach a certain phase of network growth provides a sort of "roadmap" of network development that will serve as a guide for obtaining samples with known levels of network development.

Characterizing the time-temperature transformation behavior of the epoxy amine system allows the general state of connectivity within the network to be conveniently

split into three different stages: pre-gelation, the main stage of network growth and post-vitrification. Prior to the gel point the network consists of monomer and low molecular weight oligomer and the system possesses only local connectivity. The main stage of network growth lies between the gel point and the onset of vitrification. The sample consists of a growing infinite molecular weight network during this phase of network growth. Beyond the onset of vitrification the sample consists of a well-connected network.

It is convenient to first describe the characterization of network development at a single cure temperature. This allows the general strategy and methodology of the characterization to be described in detail without complication introduced by multiple cure temperatures. This chapter, therefore, first describes the transformation behavior of a sample cured at 130°C. This temperature was chosen as it is representative of the curing temperatures typically encountered in the industrial fabrication of polymer/fiber composite parts. This same methodology is then applied to samples cured at different temperatures in order to describe the time-temperature transformation behavior of the Epon 828/3,3'-diaminodiphenyl sulfone system.

Rheological Measurement of Isothermal Transformation Behavior

As the curing reaction proceeds, the sample transitions from a low-viscosity liquid to a rubbery solid and then finally to a stiff solid. The viscosity of the sample rises and the steady-state viscosity increases rapidly as the sample nears the gel point. In fact, the steady-state viscosity becomes unmeasureable at the gel point as either the instrument overloads or the shearing force disrupts chemical bonds within the developing network. To overcome this, the rheological parameters of the system were measured in dynamic

oscillatory mode at strains low enough that it is unlikely that the measurement causes breakdown of the growing network. The gel point of the system was then determined by monitoring changes in the elastic modulus (G'), and viscous modulus (G'') of the system. The ratio of these parameters in the form of the loss tangent ($tan\delta = \frac{G''}{G'}$) expresses the relative contributions of elasticity and viscosity of a resin system. Liquid systems will exhibit a higher viscous contribution and therefore tan δ should be greater than one. Solid systems should exhibit a higher elastic contribution and therefore tan δ should be less than one. At the point where the system transitions from a liquid to a solid, that is, at the gel point, the tan δ should be expected to be equal to one. This has been found to be true for epoxy thermoset resins.[99]

While conducting measurements in dynamical oscillatory mode has the advantage of avoiding measurement-induced network breakdown, it is subject to the influence of stress relaxation processes within the sample.[100] In practice, dynamic measurement is subject to the influence of many different stress relaxation processes, each with a different characteristic relaxation time. The measurement of each relaxation process requires a measurement time on the order of the relaxation time. The effect of this is that the measured rheological properties become somewhat arbitrarily dependent on the time of the measurement (that is, the chosen oscillatory frequency). This effect can be overcome by measuring the rheological properties simultaneously at multiple frequencies to accommodate different relaxation times.

In light of these considerations, the time required for the epoxy-amine system to reach the gel point was determined by monitoring the tan δ in dynamic oscillatory mode at three different measurement frequencies. The gel point was taken to be the point at

which the measured value of tan δ was observed to be independent of the measurement frequency.[93, 94, 100] Figure 9 shows a plot of the loss tangent measured at three different frequencies as a function of cure time. The measured value of tan δ is independent of frequency after 104 minutes of isothermal cure at 130°C showing that the sample reaches the gel point after 104 minutes of cure at this temperature. This method of analysis was repeated at a variety of cure temperatures in order to characterize the temperature dependence of the time to gelation.

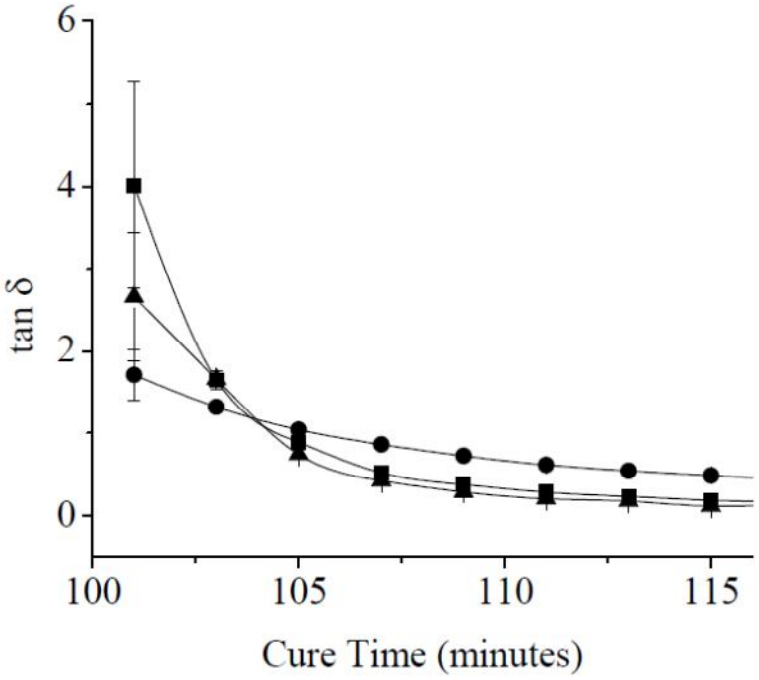

Figure 9. Tan δ as a function of cure time measured at 0.5 rad/s (■), 1 rad/s (●) and 50 rad/s (▲). The measured value of tan δ is independent of frequency at 104 minutes of cure time.

The time to the onset of vitrification in the epoxy amine system was determined by monitoring changes in the glass transition temperature of sample as a function of cure time. The glass transition temperature of a thermosetting polymer approaches the curing temperature as the sample becomes vitrified.[48, 101, 102] Unlike the gel point, the onset of vitrification is not a precise point of the network building reaction. Rather, the onset of

vitrification is approached gradually as monomer conversion increases. Due to the increasing impact of restricted diffusion on conversion, vitrification is approached gradually with time and, if enough time is allowed, the glass transition temperature of the material should be exactly equal to the reaction temperature. In practice, however, allowing the system to react long enough to allow the glass transition temperature to equal the reaction temperature is impractical for two reasons. The first reason is that the glass transition temperature asymptotically approaches the reaction temperature meaning that long reaction times would be required. The second reason is that at extended reaction times the competing influence of thermally-induced network breakdown competes with the network formation reaction in the determination of the connectivity of the molecular network, especially at higher reaction temperatures. To overcome these difficulties, this work identified the break in the linear increase of the glass transition temperature with cure time as the onset of vitrification. Admittedly, this type of analysis underestimates the true time to vitrification, however the impact of this error is not thought to significantly influence subsequent characterization as samples were tested either well before or well after this measured time to the onset of vitrification. This method provides a robust, repeatable means to determine the time to the onset of vitrification at a variety of temperatures. The time to reach vitrification can be quite long for samples cured at low temperatures (below 90°C). For these samples the time to the onset of vitrification was measured rheometrically by monitoring the time required to reach a plateau value of the storage modulus.[24] This technique is less precise than thermal characterization, so subsequent characterization was only performed on samples

cured for times significantly less than or greater than the time required to reach the onset of vitrification measured by this method.

Figure 10 shows the glass transition temperature measured by differential scanning calorimetry of a sample cured at 130°C plotted as a function of cure time. A change in slope is clearly observed at 210 minutes of cure time, corresponding to a glass transition temperature of around 125°C. This plot shows that the onset of vitrification occurs after 210 minutes of cure time. After 210 minutes of cure the reaction is essentially quenched and the system must be heated above 130°C to driver further conversion.

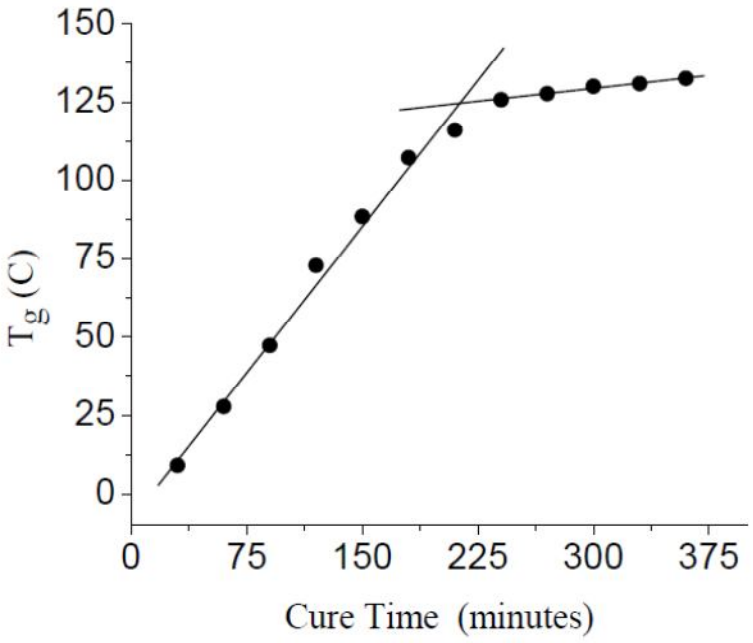

Figure 10. T_g as a function of cure time. The onset of vitrification occurs after 210 minutes of cure time.

The time to gelation and the onset of vitrification for a sample cured at 130°C is now known. This information can be used as a guide to obtaining samples with different overall network topologies. Arresting cure before 104 minutes yields a sample with no infinite molecular weight network and no connectivity. Arresting cure between 104

minutes and 210 minutes yields incomplete networks with lower degrees of connectivity near 104 minutes and higher degrees of connectivity near 210 minutes of cure. Arresting cure after 210 minutes of cure yields samples with maximum connectivity.

Time-Temperature Transformation Behavior

Similar analysis of transformation behavior at a series of reaction temperatures provides data regarding the influence of the reaction temperature on structure development. The temperature of the curing reaction plays a critical role in the way the network building reaction proceeds. Conducing an analysis of the transformation behavior at different reaction temperatures, therefore, provides a means to understand this influence on the development of connectivity within the molecular network.

The isothermal transformation behavior of the epoxy-amine system cured isothermally at temperatures ranging from 50°C up to 300°C is shown in Figure 11 and Figure 12. Figure 11 shows the amount of time required to reach the gel point. Figure 12 shows the time required to reach the onset of degradation and vitrification. Degradation was not observed within the measurement time at temperatures below 260°C.

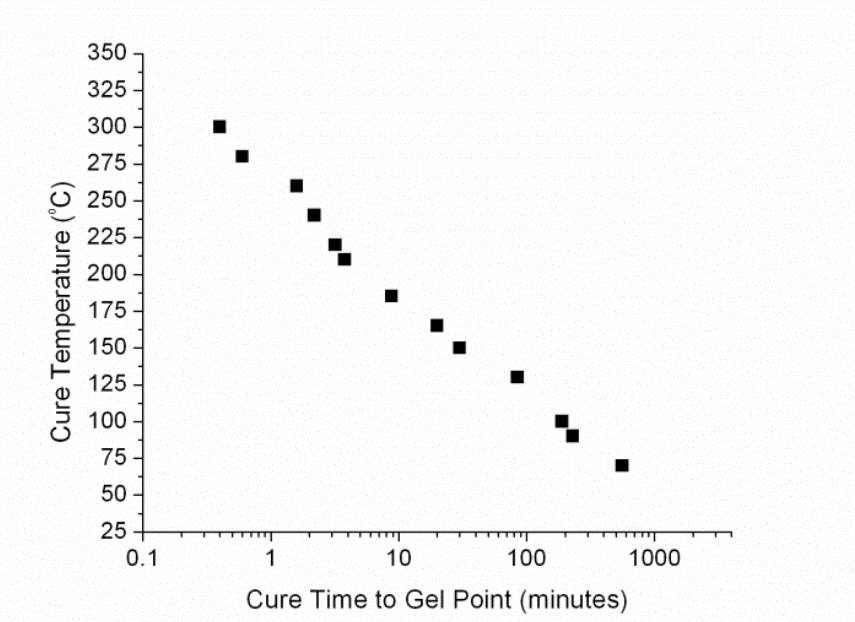

Figure 11. Cure time required to reach the gel point for a series of cure temperatures.

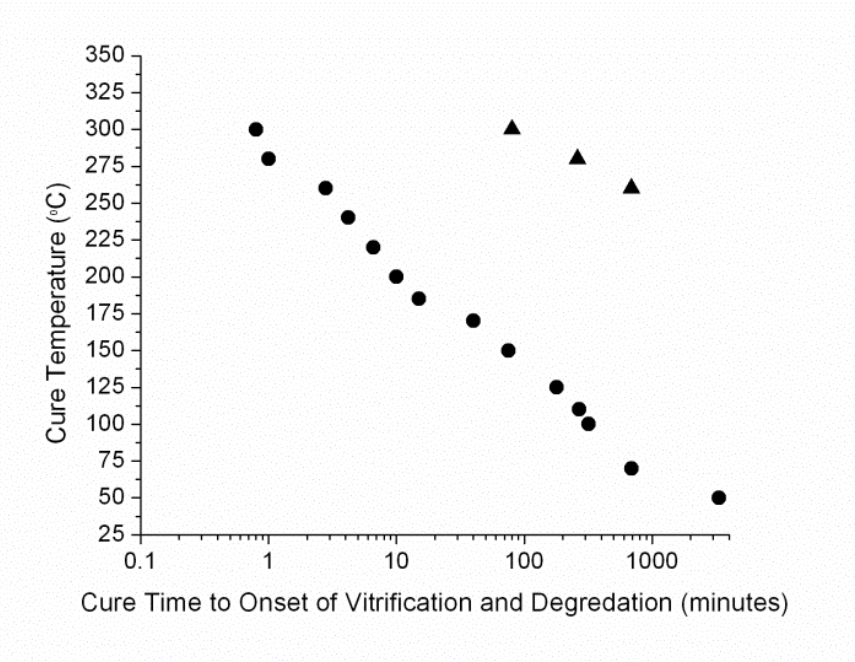

Figure 12. Cure time required to reach the onset of vitrification (●) and degradation (▲) for a series of cure temperatures.

Unsurprisingly, the time required to reach both the gel point and the onset of vitrification can clearly be seen to be dependent on the cure temperature. Samples cured

at very high temperatures were found to gel and vitrify very quickly with little time between gelation and the onset of vitrification while samples cured at low temperatures required a significant amount of time to reach the gel point and onset of vitrification. Interestingly, it was noticed that samples cured at 50°C vitrified but did not gel. This cure temperature produced a brittle, glassy solid that was entirely soluble in acetone and was found to melt at elevated temperatures in much the same way as a thermoplastic material. All other samples were insoluble, indicating the formation of an infinite molecular weight network.

In addition to providing a guideline to the state of connectivity within the network at various degrees of cure, this initial work indicated that it was unreasonable to attempt to further characterize samples cured at high temperatures, despite the fact that degradation was not observed until extended cure time. It was found that it only takes a few seconds for a sample cured at 260°C, for example, to transition from a liquid to a rubbery solid to a rigid solid. It was determined that, due to this short interval of time, it was unlikely that cure could be arrested quickly enough to produce samples with the desired level of connectivity as it takes a longer for the sample to cool than it does to transition through both the gel point and the onset of vitrification. For this reason, subsequent characterization was limited to samples cured below 200°C. This limitation has the added benefit of characterizing only samples that are less likely to have ether linkages contribute strongly to the overall network structure.

Evolution of Network Architecture During Isothermal Cure

The data presented in Figure 11 and Figure 12 provides a guide to the production of samples with various states of network development. The following is a general description of the architecture of the molecular network at each stage of network growth.

Samples cured below the gel point are in the initial, pre-gel phase of growth and have yet to develop an infinite molecular weight network. These samples are a liquid at the curing temperature however, they solidify upon cooling. Figure 10 shows a plot of the glass transition temperature of a sample cured at 130°C as a function of cure time. This plot shows that the glass transition temperature near the gel point was around 50°C and the glass transition temperature was above room temperature even around 40 minutes before gelation. It was quite simple to obtain brittle, glassy samples simply by removing the sample from the oven and cooling to room temperature. These samples showed no apparent flow even after extended times (up to a few days) although, like a thermoplastic material, they were entirely soluble in an appropriate solvent and would flow when heated above the glass transition temperature. These samples do not possess an infinite molecular weight network and are therefore poorly-connected. These samples consist of isolated domains of reacted material (gel) that are likely highly plasticized by low molecular weight and unreacted material (sol). Mass is added to the gel phase until the size of gel phase takes on the dimensions of the sample. This event is the gel point.

Samples cured beyond the gel point but not to the onset of vitrification are in the active network growth stage. Samples at this stage possess an infinite molecular weight network and unreacted species are actively being added to the growing network. Previously isolated gel domains as well as unreacted species are added to the growing

network during this phase. The gel point at the beginning of this stage of network growth also marks the first point where diffusion control begins to play a role in development of the network structure. The infinite molecular weight network is only lightly developed at the gel point and therefore restricts the diffusion of only the largest isolated gel domains. As the network increases in mass, smaller and smaller species become diffusion restricted by the increasingly-connected molecular network. The existing network, therefore, does not have a constant influence on the addition of mass as only the largest species are influenced initially while smaller unreacted species can more easily diffuse through the growing network. This non-constant influence of the network on its own development may be reasonably assumed to play a role in the development of non-homogeneity within the network structure.

Samples cured to the onset of vitrification have a crosslink density high enough to restrict the diffusion of unreacted species to active reaction sites. Network development has effectively stopped by this stage of the curing reaction and elevated temperatures are needed to enable diffusion of unreacted species to active reaction sites.

CHAPTER VII

TOPOLOGY OF THE EPOXY-AMINE NETWORK

Chapter Overview

The topology of the crosslinked epoxy-amine molecular network is function of the molecular connectivity of the network. While the rheometric and thermal characterization discussed in the previous section provides a valuable general understanding of the development of molecular connectivity within the network, it lacks the resolution needed to characterize molecular-scale connections within the network. Real time near-infrared spectroscopy (NIR), on the other hand, is capable of monitoring the development of segment connections within the network during the curing reaction. Rheometry, thermal characterization and spectroscopic analysis are complimentary techniques in the analysis of molecular network architecture. Rheometric and thermal analysis provides information about the global connectivity of the molecular network while NIR provides information about the average molecular connectivity within the network.

Near-infrared spectroscopy provides two different types of information about the topology of the developing network. First, NIR reveals the relative concentration of primary, secondary and tertiary amine therefore showing the "average" topology of the molecular network – that is, NIR can show if the network is mostly unconnected, mostly linear, or mostly branched or crosslinked by revealing the relative concentration of each amine species. Second, NIR is capable of providing information about the relative rate of production of each amine species. Figure 13 shows a schematic of two different samples at the gel point. Figure 13a shows a system that produces linear segments much faster

than branched segments. Figure 13b shows a system that produces linear and branched segments at nearly the same rate. The fast production of linear segments is expected to produce a mostly-linear network similar to that shown in Figure 13a. Similar rates of production of linear and branched segments is expected to produce networks with a higher number of loops and other intermolecular connections prior to gelation and therefore produce a network similar to that shown in Figure 13b. Which type of behavior is exhibited by the system is dependent on the reactivity ratio of the primary versus secondary amine. If the first functional group is more likely to react than the second, the linear structure shown in Figure 13a would be more likely to form. If both groups show equal reactivity, the structure shown in Figure 13b would be more likely to form. This chapter will show that the reactivity of the amine curing agent in the Epon 828/3,3'-diaminodiphenyl sulfone system studied here influences the connectivity of the molecular network and that this difference in reactivity is temperature dependent. A subsequent section will show that this temperature dependence can, in fact, be used to tune to the nanoscale morphology of the network.

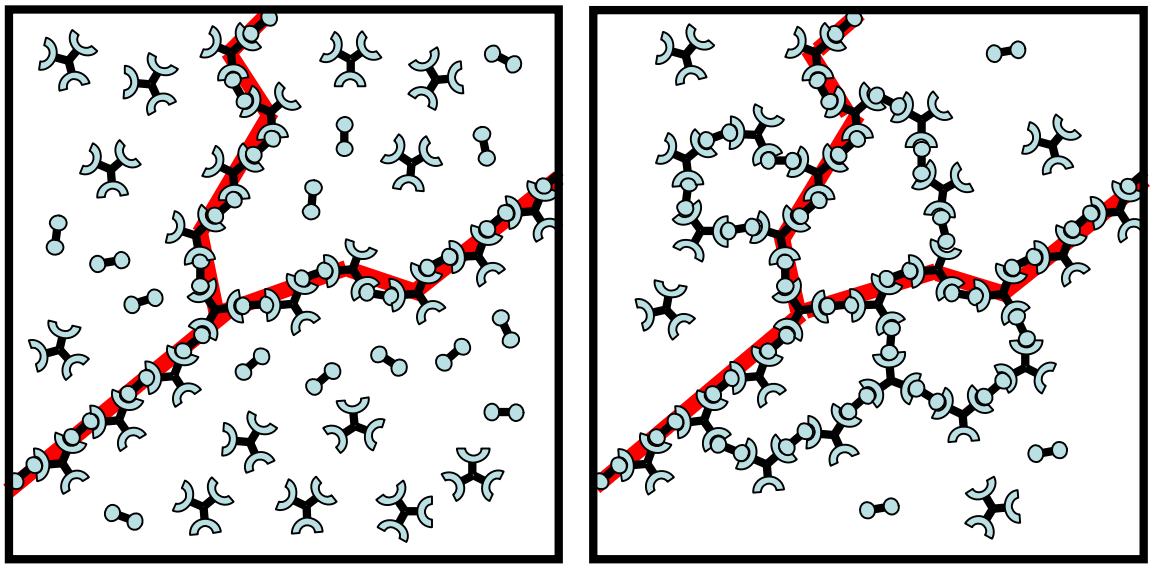

Figure 13. Two different modes of network growth. Network growth similar to that shown in Figure 13a (left) is expected if the primary amine is more reactive. Network growth similar to that shown in Figure 13b (right) is expected if the primary and secondary amine species show similar reactivities.

Each amine moiety on the DDS monomer participates in two distinct reactions during cure. The primary amine will first react with an epoxide to produce a secondary amine which in turn reacts to form a tertiary amine. The reaction of the primary amine results in a linear segment while the subsequent secondary amine reaction produces either a branch or a crosslink, depending on prior connectivity. This type of incremental network growth means that each network building step takes place in a slightly different chemical and physical environment. It is possible for the reaction of the secondary amine to be catalyzed by the presence of the nearby hydroxyl group that results from the ring opening reaction of the epoxide group during the reaction of the primary amine, especially at lower reaction temperatures. Additionally, this prior linkage introduces a degree of steric hindrance than may influence the addition of another monomer unit during the reaction of the secondary amine. The effect of these effects is that the primary and secondary amine will show different reactivities.

Development of the Epoxy-amine Network Topology

As before, it is convenient to first consider the results of NIR analysis for a single reaction temperature. The non-normalized NIR absorption spectra of the Epon 828/DDS system at six selected levels of cure at 130°C is shown in Figure 14. This spectra is typical of spectra for all cure temperatures. The location of the assigned absorption bands is in good agreement with those reported in the literature.[26, 37, 103] Two peaks characteristic of oxirane can are seen: a broad peak at 5760-6100 cm^{-1} and a sharper peak at around 4540-4550 cm^{-1} (convoluted with the primary amine). The broad peak is attributed to the first overtone of the terminal CH_2 in the stretching mode while the sharper peak is due to a combination of the second overtone of the epoxy ring with the fundamental C-H stretch.[104, 105] A non-convoluted primary amine band can be seen at 5040-5110 cm^{-1} as a strong peak with a small shoulder. The strong peak is attributed to a combination of the NH stretch at 3464 cm^{-1} and NH bend at 1630 cm^{-1}. The shoulder is attributed to a combination of the asymmetric stretch at 3367 cm^{-1} and the same bend at 1630 cm^{-1}.[104] The secondary amine appears at 6610-6750 cm^{-1}, convoluted with the primary amine. This broad peak is attributed to the asymmetric NH stretch at the lower end of the integration range and symmetric NH stretch at the higher end of the integration range. The absorbances were deconvoluted according to the procedure described in the experimental section. Absorbance of the hydroxyl group occurs just beyond that of the secondary amine and occurred as a very broad peak and is not shown here. Reasonably constant absorbance of the phenyl rings can be seen at 4610-4690 cm^{-1}. This absorbance is attributed to the aromatic C-H stretch.[26] Variation in area of this range is due to

sample-to-sample variation in path length. Each spectrum was normalized to the original spectrum taken at zero cure time using the measured absorbance at this integration range.

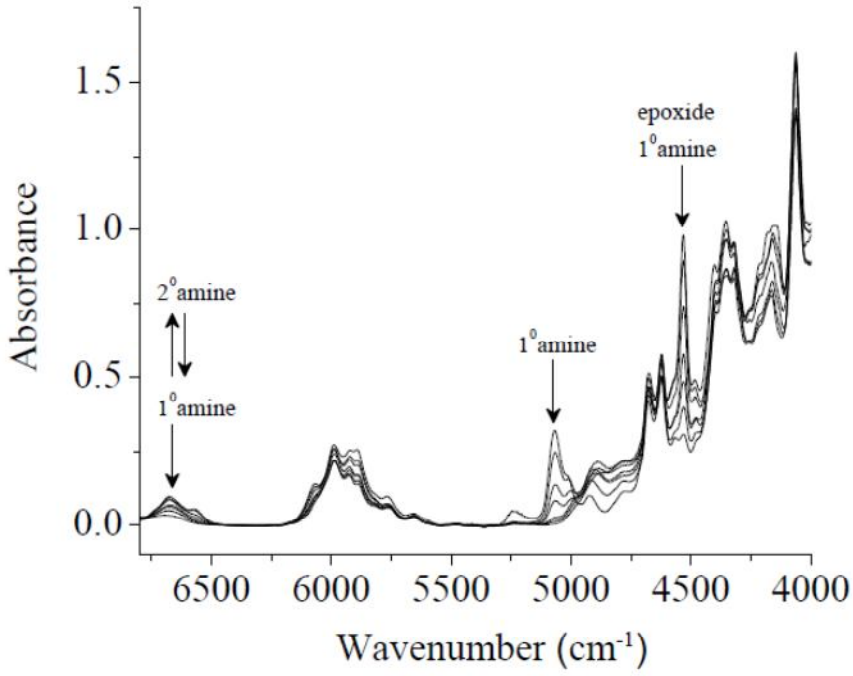

Figure 14. Near-infrared spectra of stoichiometric Epon 828/DDS mixtures at 0, 50, 94, 104, 144 and 234 minutes of cure showing epoxy conversion (4540-4550 cm^{-1}), primary amine conversion (5040-5110 cm^{-1}) and formation and subsequent conversion of the secondary amine (6610-6750 cm^{-1}). Arrows indicate change in absorbance as cure progresses. The phenyl absorbance used as the internal standard can be seen at 4610-4690 cm^{-1}.

The concentration of each species can then be found by integrating the peak area and relating absorbance to concentration according to Beer's law. This procedure is outlined in the experimental section. The concentration of each species can then be plotted as a function of cure time to illustrate changes in the relative during the network building reaction. The concentration curve from the sample cured at 130°C is shown in Figure 15. The gel point and onset of vitrification, as measured by rheometry and differential scanning calorimetry, respectively, are also indicated.

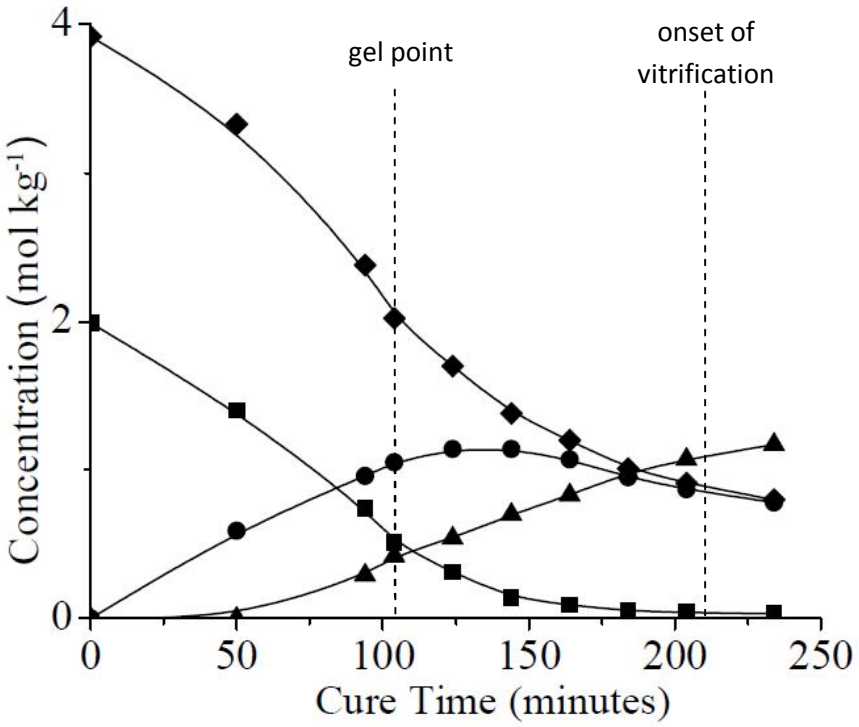

Figure 15. Concentration of epoxide (◆), primary amine (■), secondary amine (●), and tertiary amine (▲) chemical groups as a function of cure time. The initial concentration of primary amine is half the concentration of epoxide as each primary amine has two active reaction sites.

Understanding the relationship between the detected amine species (that is, primary, secondary or tertiary) and the consequent molecular linkage (none, linear, branched/crosslinked, respectively) allows the concentration curve to be interpreted in such a way as to reveal the molecular architecture of the network at various stages of the network building reaction. This plot shows that for samples cured at 130°C. The major chemical change during the pre-gelation stage of network development at this temperature is the conversion of primary amine to secondary amine to produce a linear segment. A minor amount of branching or crosslinking occurs during this stage of network development as evidenced by the appearance of tertiary amine at cure times greater than 50 minutes. The predominant molecular architecture during the pre-gel

phase of network development, therefore, is mostly-linear oligomers with occasional branches or crosslinks. This oligomeric material increases in mass until the gel point, when it links together to form a mostly-linear, infinite molecular weight network. The concentration of secondary amine continues to increase after the gel point but reaches a maximum early in the active network growth stage of the reaction. The dominant reaction during the active stage of network growth is the conversion of secondary amine to tertiary amine – the crosslinking reaction. Essentially all of the primary amine has reacted by the midway point of the second phase of network growth, therefore most network development after this point results from intra-network crosslinking reactions rather than the addition of unreacted monomer to the network. Tertiary amine is the dominant species during the vitrification stage of network growth. The high amount of crosslinking after vitrification restricts the ability of unreacted species to diffuse to active reaction sites. Analysis of epoxide concentration shows that for this curing regimen the samples do not reach a high degree of conversion prior to the onset of vitrification – only around 75% of the epoxy groups are consumed during the reaction. An elevated temperature post-curing step is required to drive the curing reaction to higher conversion.

A general description of the development of the molecular network can now be developed for samples cured at 130°C. Monomer units assemble into mostly linear structures during the initial, pre-gelation stage of network development, as evidenced by the increasing concentration of secondary amine during this phase. Little tertiary amine, which is indicative of branched or crosslinked structure, depending on prior connectivity, is detected until later stages of the network building reaction. The mass of these mostly-linear structures increases up to the gel point, where they link to form an infinite

molecular weight “skeleton network”. Mass is then added to this network during the main stage of network growth as the secondary amine is consumed to produce crosslinks. The main stage of network growth is characterized by crosslinking of the initial “skeleton network”. This mode of network growth continues to the onset of vitrification.

Temperature Dependency of Linkage Development

Similar analysis of samples cured at different temperatures reveals the influence of the reaction temperature on the mode of molecular network development. Figure 16 shows concentration curves of primary, secondary and tertiary amine species as a function of cure time for samples cured at 90°C, 150°C and 185°C up to the onset of vitrification. The effect of cure temperature on the conversion of monomer can be clearly seen in these figures. At 90°C (Figure 16a), concentration changes linearly for all amine species. The concentration of tertiary amine increases nearly concurrently with the concentration of secondary amine. At 150°C (Figure 16b), the concentration of secondary amine increases quickly to reach a maximum concentration after around 50 minutes of cure. Tertiary amine conversion shows an apparent induction period with little tertiary amine produced until approximately 75% of the primary amine has been converted to secondary amine, similar to sample cured at 130°C discussed earlier. At 185°C, primary amine shows nearly complete conversion within 20 minutes. The secondary amine again shows a maximum concentration, although only about one-third of the maximum concentration achieved at 150°C. Interestingly, the concentration of tertiary amine increases nearly concurrently with secondary amine concentration during the first five minutes of cure, similar to the conversion behavior observed for the sample

cured at 90°C. That is, primary and secondary amine is produced at similar rates for samples cured at 90°C and 180°C, but not for samples cured at 150°C.

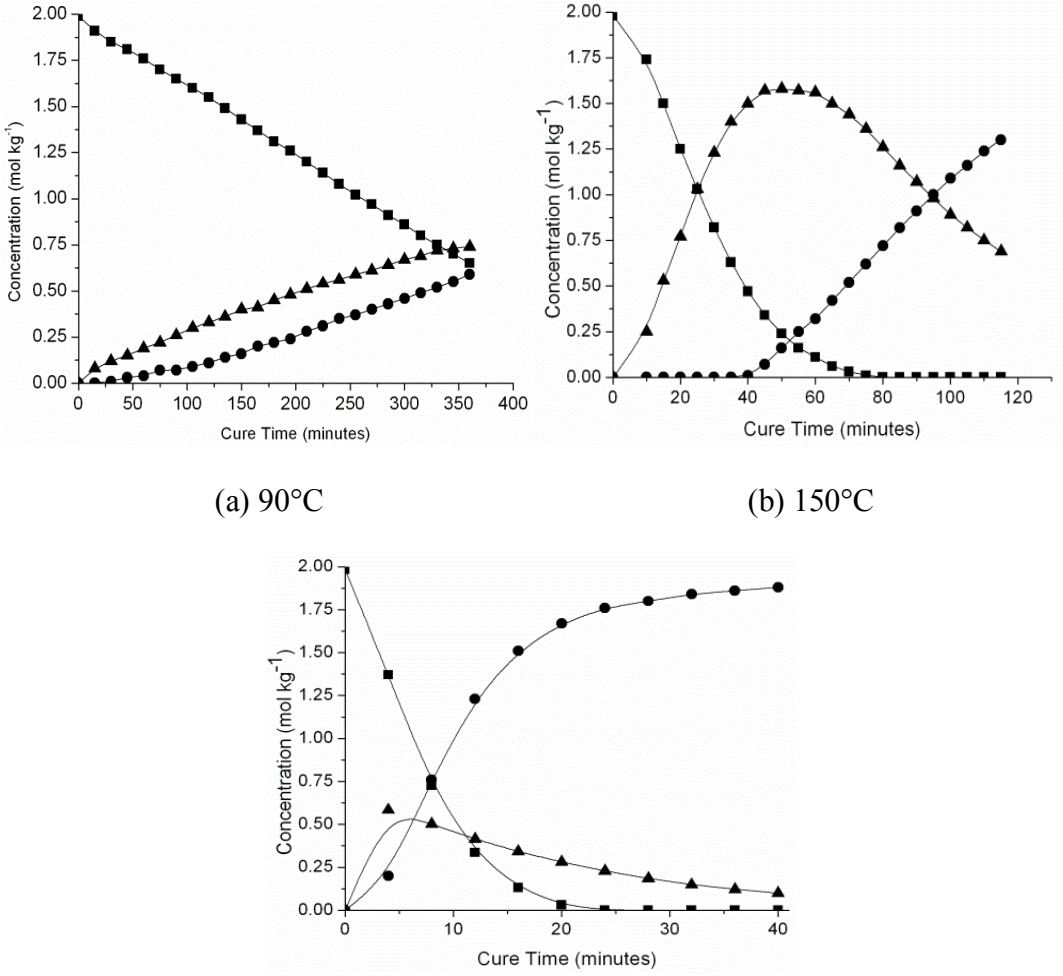

(a) 90°C (b) 150°C

(c) 185°C

Figure 16. Concentration of primary amine (■), secondary amine (▲) and tertiary amine (●) as a function of cure time. 18a: 90°C, gel point at 231 minutes, vitrification at 316 minutes, final epoxy conversion was 49%. 18b: 150°C, gel point at 30 minutes, vitrification at 75 minutes, final epoxy conversion was 84%. 18c: 185°C, gel point at 9 minutes, vitrification at 15 minutes, final epoxy conversion was 94%.

Determining the ratio of linear segments compared to the number of branched segments is particularly helpful for understanding how the network grows during the initial pre-gelation stage of network development. This method is advantageous as the

rates of linear and branched segment production can be measured directly from the plots in Figure 16. This rate is distinct from the chemical conversion rate of the amine species, which, as was shown, can be quite complicated to determine. The rate of production of each type of connection point is a direct measurement from the conversion curves shown in Figure 16 and is not complicated by the need to consider the action of autocatalytic behavior, differences in primary and secondary amine reactivities, and the non-instantaneous shift from chemical to diffusion control. The production rate of linear and branched/crosslinked segments depends only on the change in the measured concentration as a function of cure time and no rate equation is necessary for its determination. At these reaction temperatures, it is assumed that the epoxy-amine reaction is the dominant network forming reaction.[25]

Table 2 shows the production rate of linear segments and branched/crosslinked segments during the pre-gelation stage of network development. These values were calculated from the initial slope of the concentration of secondary and tertiary amine plotted in Figure 16. Comparison of the rates of production of secondary and tertiary amines reveals differences in the molecular architecture of the nanogels formed during the initial stages of the cure reaction. As expected, overall segment production rates are found to increase with increasing temperature. However, the relative rate of production of linear segments and branched/crosslinked segments within a sample is seen to vary with temperature. Samples cured at 185°C produce linear and branched/crosslinked segments at about the same rate, at 90°C linear segments are produced approximately twice as fast as branched/crosslinked segments while samples cured at 150°C produce linear segments more than ten times faster than branched/crosslinked segments. The

seemingly contradictory behavior of faster relative secondary amine production at both lower and higher temperatures may be explained by the discussion of the influence of auto-catalysis at lower temperatures and the similar reactivity of the primary and secondary amine at higher temperatures presented in Chapter II.[32, 47]

Table 2

Rate of development of linear and branch/crosslink segments during the pre-gelation stage of cure as determined by rate of production of secondary amine (linear segment) and rate of production of tertiary amine (branch/crosslink).

Segment	90°C	150°C	185°C
Linear	0.0037 mol kg^{-1} min^{-1}	0.0403 mol kg^{-1} min^{-1}	0.1398 mol kg^{-1} min^{-1}
Branch/Crosslink	0.0014 mol kg^{-1} min^{-1}	0.0031 mol kg^{-1} min^{-1}	0.1115 mol kg^{-1} min^{-1}

Comparing segment production rates shows that samples cured at 150°C produce initial nanogels with a mostly-linear molecular structure while the initial nanogels produced in samples cured at 90°C and 185°C take on a more crosslinked or branched molecular architecture. These different molecular development behaviors are likely responsible for observed differences in fracture surface morphologies. Figure 17 shows a schematic that illustrates the influence of this behavior on the likely growth of the network. The image at the top shows initial linear growth up to the gel point, where the linear molecules link to form a more-homogeneous network structure. The image at the bottom shows the type of network growth associated with equal rates of production of linear and crosslinked segments. This type of network growth indicates the formation of gel particles prior to gelation that link together at the gel point to form a less-

homogeneous network structure. This type of development is quite similar to that predicted by Labana, Chompff and Newman in their statistical treatment of the formation of "gel balls" within the architecture of cured thermoset networks.[56] Relatively fewer crosslinks are produced at moderate temperatures, allowing the growing gel particles to better retain their linear structure up to the gel point. At higher and lower temperatures relatively more crosslinks are produced, restricting the conformations available to the growing chains and encouraging the further production of intramolecular crosslinks.

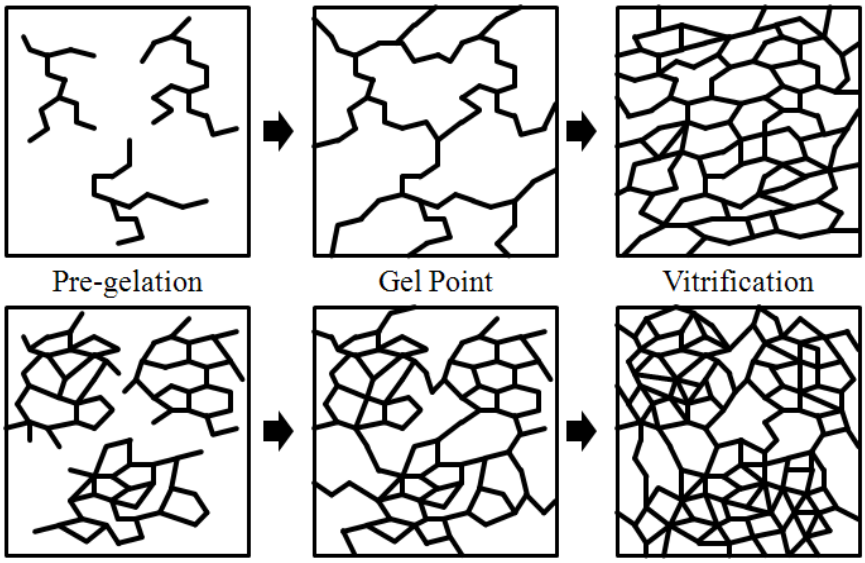

Figure 17. Schematic illustrating two different types of network growth. Growth typified by the top schematic will yield more homogeneous networks than that of the bottom schematic.

CHAPTER VIII

THE HETEROGENEOUS ARCHITECTURE OF THE EPOXY-AMINE MOLECULAR NETWORK

Chapter Overview

The rheological, thermal and spectroscopic studies conducted by this work provide valuable information about the general state of the network. Studies of the time-temperature transformation behavior of the system reveal the state of global connectivity within the system while spectroscopic analysis reveals the average state of the molecular connectivity. Spectroscopic analysis of the relative rates of primary and secondary amine conversion has demonstrated that, at certain temperatures, the network building reaction favors the formation of a non-homogeneous structure much like the formation of "gel balls" that was predicted by Labana, Chompff and Newman.[56]

This chapter presents the results of AFM interrogation of critical fracture manifolds. First, critical fracture manifolds from each stage of network development obtained from a sample cured at 130°C are presented to demonstrate the development of non-homogeneity in the architecture of the network during the network building reaction. Then, a series of AFM images of the critical manifolds of epoxy-amine networks formed at different reaction temperatures is presented to demonstrate the influence of cure temperature on the architecture of the molecular network. This chapter concludes with a brief analysis of the influence of differences in these architectures on their ability to resist fracture propagation.

Cure-Time Dependence of the Critical Fracture Manifold

Figure 18 shows topographic and phase AFM images obtained from fracture surfaces of a sample cured at 130°C at increasing amounts of cure time. Each of the three stages of network development yields a different fracture surface morphology. Figure 18a, obtained from a sample in the initial pre-gelation stage of cure, shows the featureless, planar fracture surface typical of samples with low levels of network development. Figures 18b, 18c and 18d, obtained from samples in the main stage of active network growth, exhibit the nodular nanostructures typical of epoxy-amine systems. These nanostructures are first observed in samples taken at the gel point (Figure 18b) and appear more regular in samples taken near the onset of vitrification (Figure 18d, sample taken 20 minutes prior to the onset of vitrification). Figure 18e, obtained from a sample taken shortly after the onset of vitrification, shows a change in the fracture surface morphology, as the nodular nanostructures appear less defined in the topography image (left) and the surface is much rougher.

AFM phase imaging provides information about the distribution of mechanical and viscoelastic properties of the network near the fracture surface by monitoring the way in which the oscillating tip interacts with the sample. Changes in this interaction, however, are also influenced by variation in the tip/sample contact area during scanning which affects the total amount of force applied to the surface by the oscillating tip. [106, 107] This variation will cause non-network effects such as edges and sharp surface gradients to disproportionally affect the tip/sample interaction. The phase images in Figure 18 show that variation in the measured phase lag is concentrated in the region between nanostructures where the slope of the surface topography changes sharply. For this

reason, it cannot be definitively stated that the measured phase lag is solely a result of differences in viscoelasticity between the central region of the nodule and the interstitial region.

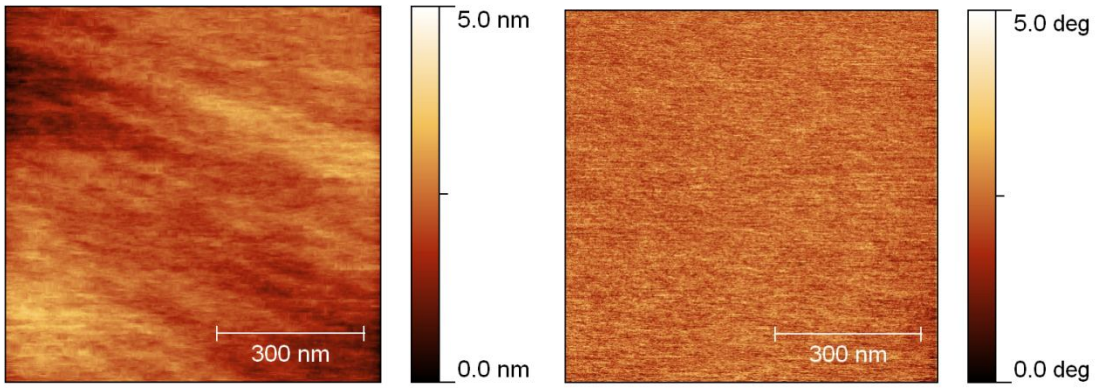

(a)

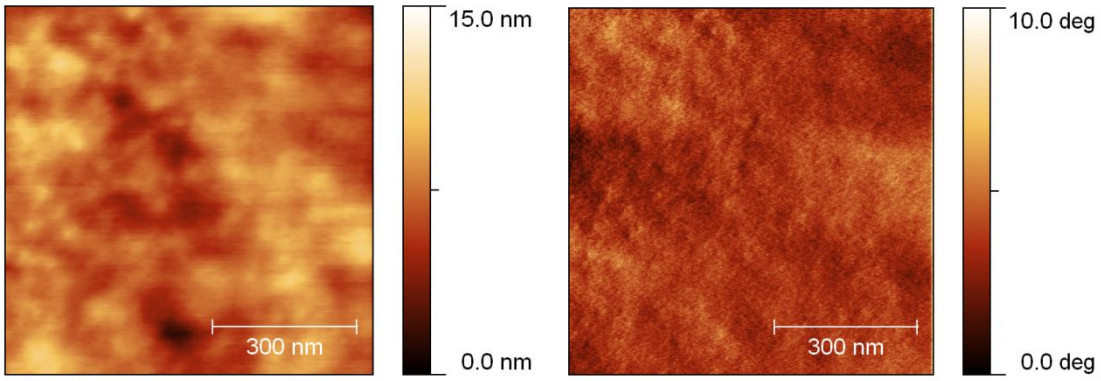

(b)

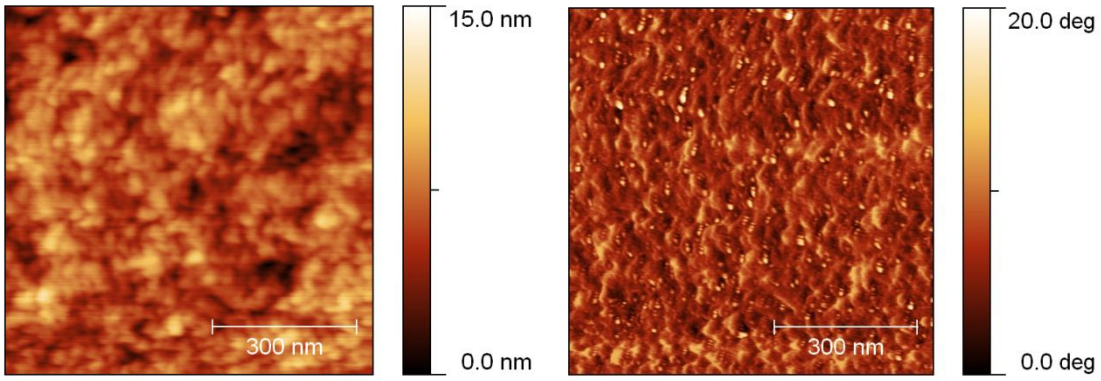

(c)

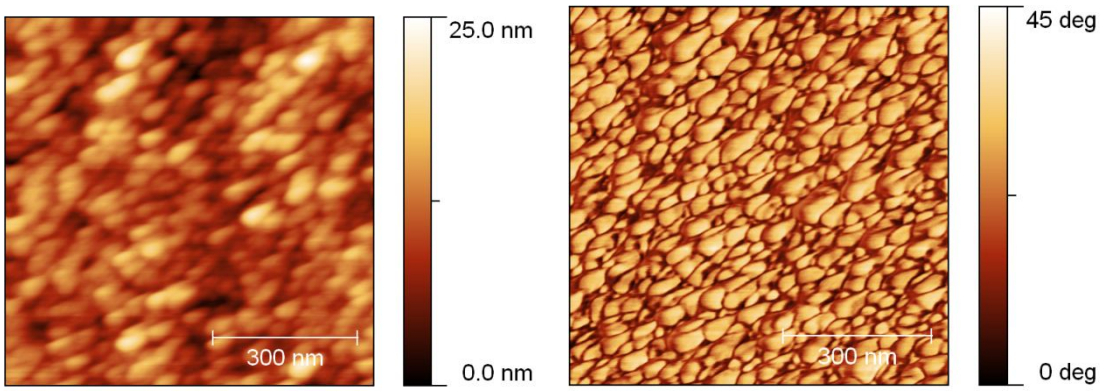

(d)

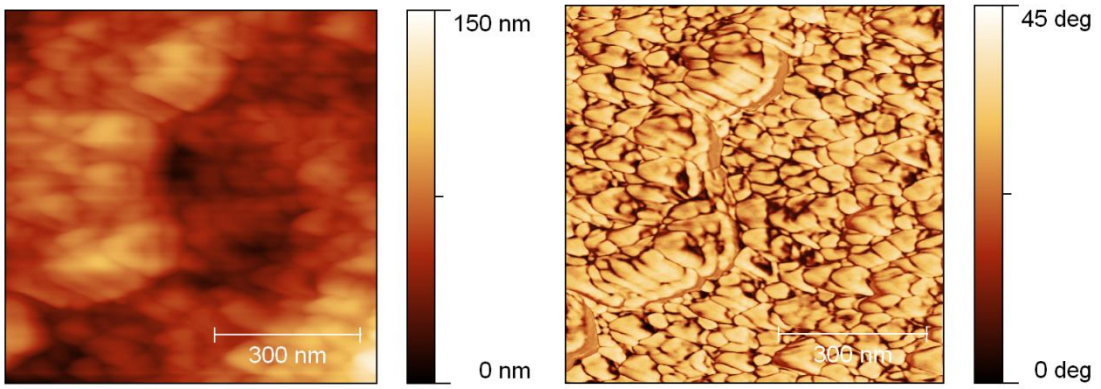

(e)

Figure 18. AFM topographic (left) and phase (right) images of the fracture surface of the epoxy-amine system at various stages of cure. Each image represents an area 750nm x 750 nm. (a) 84 minutes (pre-gelation), (b) 104 minutes (gel point), (c) 124 minutes (active growth stage), (d) 184 minutes (active growth stage) and (e) 224 minutes (post-vitrification). Each image is 750 nm × 750 nm. Cure temperature: 130°C.

The Influence of Plastic Deformation on the Ability to Use the Fracture Pathway as an Indication of Nonhomogeneous Crosslink Distribution

The issue of plastic deformation must be addressed before the fracture pathway can be used as an indicator of the underlying structure of the crosslinked molecular network. The morphology of the fracture surface cannot be used to discern network structure if the observed morphology is simply a consequence of the fracture process. Samples must undergo brittle fracture with little plastic deformation. The creep characteristics of the fracture surfaces were determined by nanoindentation in order to

understand each sample's resistance to plastic deformation at the scale of the individual nanostructures. This was done by applying a static load to the fracture surface while monitoring tip displacement over time. Figure 19 shows that that, as expected, samples cured for lower amounts of time show a higher amount of flow in response to an applied force. If the observed nodular morphology was a result of flow during the fracture process, it would be anticipated that the lowest cured samples would be most likely to exhibit the nodular morphology. The AFM images in Figure 18 show, however, that this is not the case. Another possibility that must be considered is that flow of the surface material at the nanoscale could conceivably allow the morphology of the fracture surface to change during the time interval between fracture and AFM imaging. Figure 20 shows a 30nm deep indentation made at the fracture surface of a sample where cure was arrested 20 minutes prior to gelation. No recovery of the indentation is observed even after 120 minutes of continuous imaging indicating that flow does not occur in the samples within time scales that are important for this work. These indentation studies indicate that flow processes and plastic deformation are not expected to significantly influence the morphology of the fracture surface.

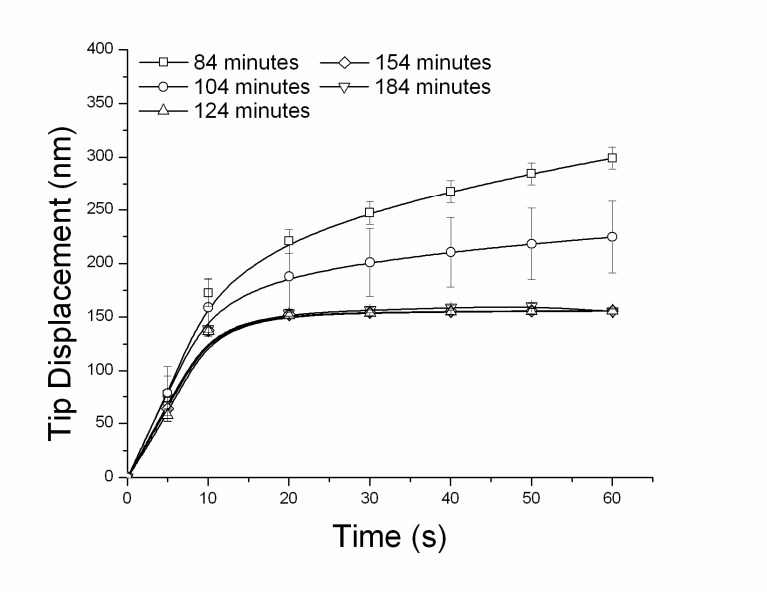

Figure 19. Tip displacement as a function of time under constant load for samples with increasing lengths of cure time.

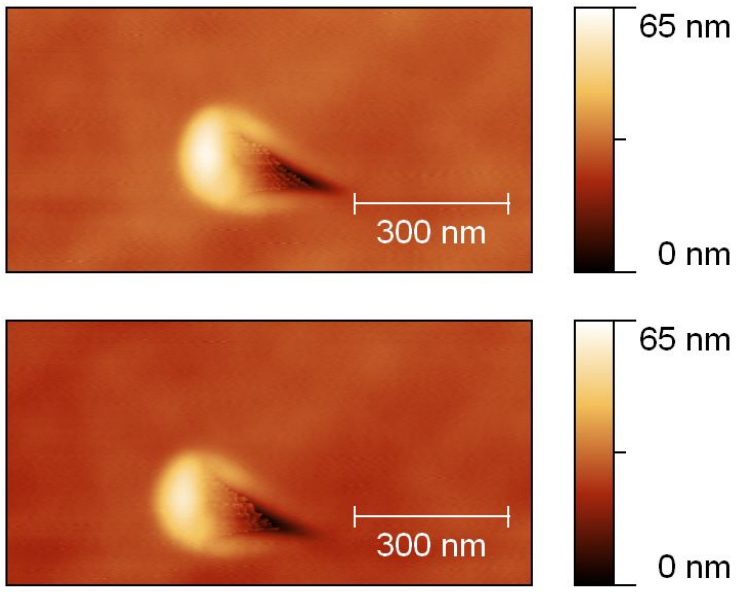

Figure 20. Topographic AFM image nanoindentation produced on surface of sample cured at 130°C for 84 min (20 minutes before gelation). This cure time produces a glassy sample. No change is seen in the indentation in images taken immediately after indentation (top) and 120 min after indentation (bottom).

Evolution of Network Connectivity in the Epoxy Amine System During the Network Building Reaction

AFM interrogation of the critical fracture manifold at increasing degrees of network development can be used in conjunction with NIR analysis of amine conversion to provide a way to understand the nanoscale distribution of crosslink density during the curing reaction of the epoxy amine system. Figures 21a-e show three-dimensional projections of topographic AFM images of fracture surfaces taken at increasing levels of cure for the sample cured at 130°C. Profiles extracted from the regions marked in black are shown alongside the images. It can be seen that differences in the level of network development influence the fracture pathway of the propagating crack tip. The RMS roughness values from each image are plotted in Figure 22 as a function of cure time as a means of quantifying the deviation of fracture surface from planarity with increasing curing time.

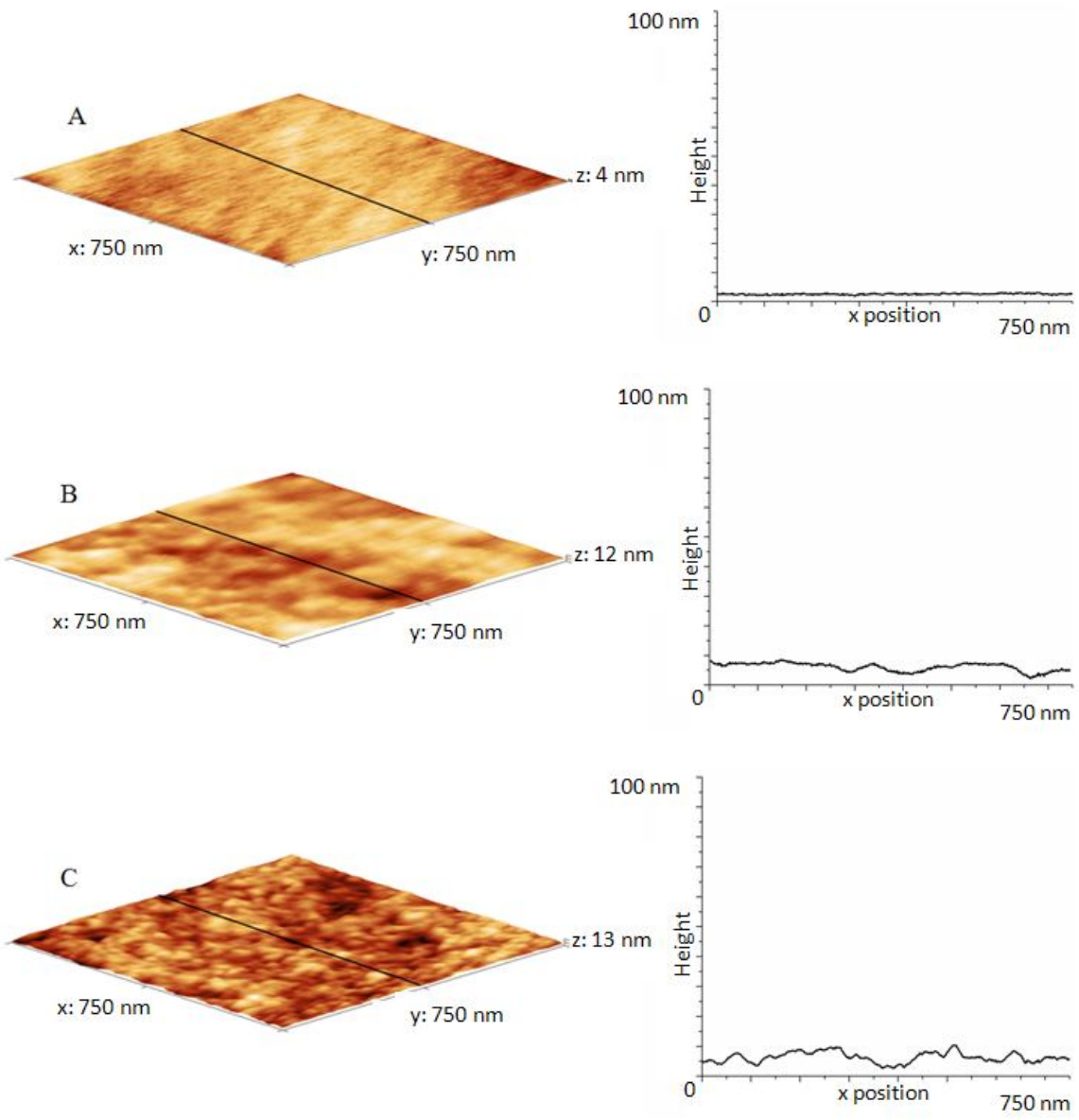
A
z: 4 nm
x: 750 nm
y: 750 nm
100 nm
Height
0
x position
750 nm
B
z: 12 nm
x: 750 nm
y: 750 nm
100 nm
Height
0
x position
750 nm
C
z: 13 nm
x: 750 nm
y: 750 nm
100 nm
Height
0
x position
750 nm

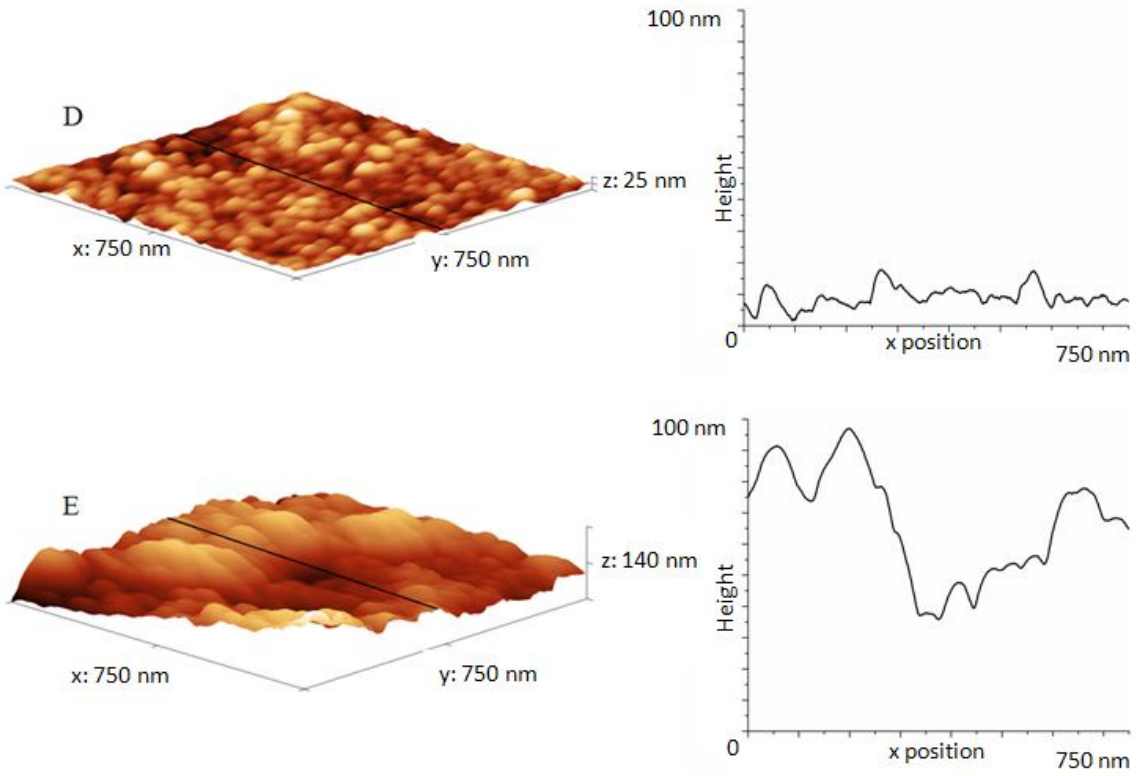

Figure 21. Topographic AFM images of the fracture surface of the epoxy-amine system at various stages of cure: (A) 84 minutes, (B) 104 minutes (gel point), (C) 124 minutes, (D) 184 minutes and (E) 224 minutes. Cure temperature: 130°C. AFM images are presented with a 1:1:1 aspect ratio while surface profiles are shown on identical z-scales.

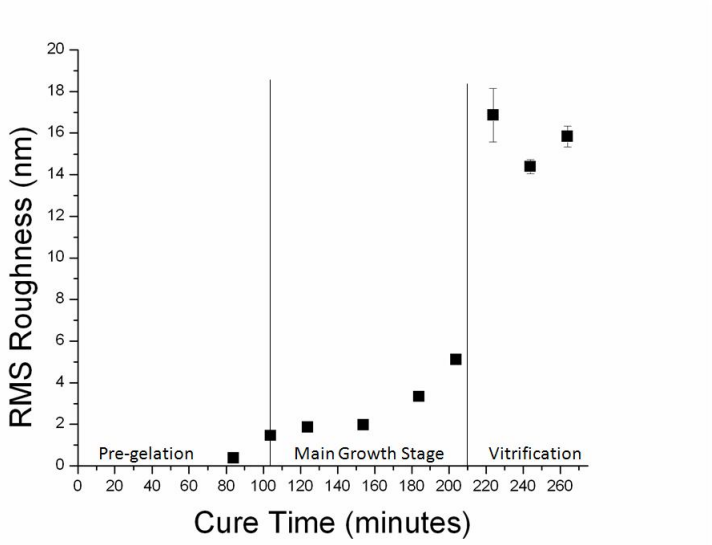

Figure 22. RMS Roughness values of the fracture surface of a series of epoxy-amine fracture surfaces as a function of cure time. Cure temperature: 130°C.

Figure 21a shows a representative AFM image of a sample during the pre-gelation stage of network development. The sample was removed from the oven and allowed to cool below the glass transition temperature prior to fracture. This image shows the highly planar fracture surface indicative of a homogeneous underlying structure. The planar fracture behavior means that the system has a homogeneously low level of crosslinking; the critical fracture manifold does not indicate any regions with a relatively higher degree of crosslinking. Oligomeric regions have a higher amount of crosslinking than unreacted monomer but these regions did not appear to influence the way in which the crack tip propagated through the sample. The low number of covalent bonds in these areas may not provide a significant barrier to propagation or these regions may be so highly plasticized by unreacted monomer that they are easily pushed aside by the propagating crack tip.

Fracture surfaces of samples fractured during the stage of active network growth are shown in Figures 21b-d. The development of the nanostructures during the main

stage of network growth can be clearly tracked in these images. Figure 21b shows that the nodular nanostructures first appear at the gel point. NIR analysis shows that the sample in 23b consists mostly of a linear network, however, an appreciable amount of tertiary amine has developed indicating the presence of some crosslinking. The concentration of tertiary amine continues to increase during the stage of active network growth as the nodular nanostructures become more regular and well-defined as seen in Figures 21c and 21d. This relationship between tertiary amine concentration and morphological development indicates that the developing network consists of nodular regions of relatively higher crosslink density approximately 50 nanometers in size during the main stage of network growth. Neither the number nor size of the nodular nanostructures increases appreciably during this phase of the reaction which indicates that the majority of the crosslinking reaction occurs within individual nanostructures. The nodules do not appear to coalesce into larger structures.

Figure 21e shows an image taken on the fracture surface of a vitrified sample. This image shows a significantly rougher fracture surface. NIR analysis shows that tertiary amine is the dominant amine species meaning that the majority of the network has some degree of crosslinking. The clearly defined nodules seen in 23d have mostly disappeared. The plot of RMS roughness in Figure 22 shows a sharp increase at the onset of vitrification. This dramatic increase in roughness indicates that the crack tip deviates strongly in order to follow a low energy propagation pathway. This increase in RMS roughness as well as the loss of the clearly-defined nodular morphology can be explained by an increase in inter-nodular crosslinking that prevents the crack tip from simply propagating around individual gel particles as it does during the main stage of network

growth. Rather, because of the increased internodular crosslinking after the onset of vitrification, the propagating crack tip propagates around clusters of nodules.

Temperature-Dependence of the Critical Fracture Manifold

Topographic AFM images of fracture surfaces of the epoxy-amine system cured at different temperatures are shown in Figure 23. These samples were cured isothermally up to the onset of vitrification. RMS roughness values of these images are plotted in Figure 24. Figure 23a, cured at 50°C, shows the fracture surface of a sample that vitrified without gelling. This surface appears similar to that observed in AFM images taken of samples where cure had been arrested prior to gelation (Figure 18a). The RMS roughness is quite low, indicating that the surface is planar. This high planarity is due to the lack of an infinite weight molecular network to present a barrier to crack tip propagation. Figure 23b from a sample cured at 90°C distinctly shows the nodular morphology commonly observed in epoxy systems. This sample consists of crosslinked nodules around 50 nm in diameter surrounded by an interstitial region that likely contains a high concentration of unreacted material as overall conversion is very low (49% epoxy conversion). Figures 23c and 23d, cured at 110°C and 130°C, respectively, show similar morphology and significant increases in surface roughness. These two morphologies illustrate the transition from the distinct, regular nodular structures seen in the sample cured at 90°C to the very rough fracture surface found in samples cured at 150°C. It is difficult to discern nodular structures in Figure 23e, cured at 150°C. Rather, a very rough fracture surface is observed. Figure 23f shows the fracture surface morphology of a sample cured at 185°C. The nodular nanostructures are observed, although they appear

less distinct and smaller in diameter (only around 30 nm) in comparison to those observed at lower cure temperatures.

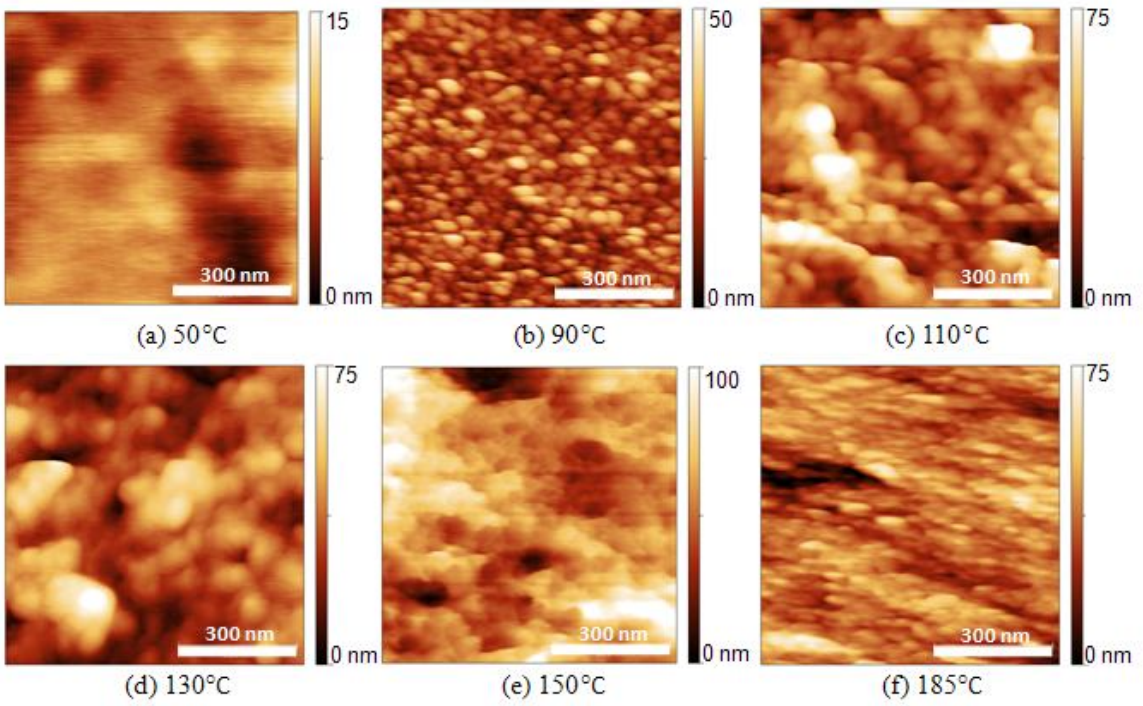

Figure 23. Topographic AFM images of samples isothermally cured to the onset of vitrification at various temperatures.

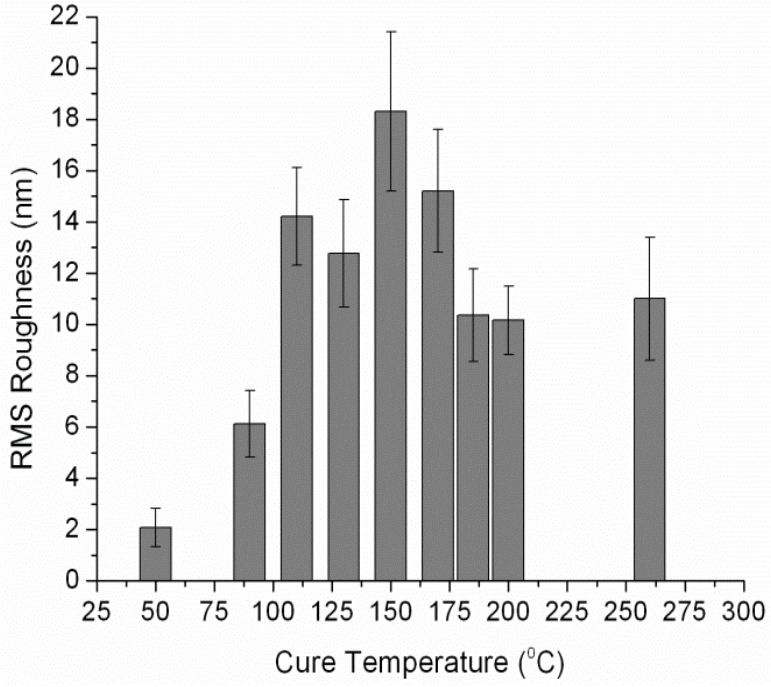

Figure 24. RMS roughness of the fracture surface of samples isothermally cured to the onset of vitrification at various temperatures.

Interpreting the cure temperature dependent morphology of these fracture surfaces in light of the differences in the initial molecular architecture as determined by NIR analysis provides insight into the influence of cure temperature on structure development. Both Figure 23b, cured at 90°C, and Figure 23f, cured at 185°C, show regions of higher crosslink density surrounded by an interstitial region of relatively lower crosslink density. Figure 23e, cured at 150°C, does not show the well-defined nodular structure. NIR analysis showed that samples cured at 90°C and 185°C develop linear and crosslinked segments nearly simultaneously, while the sample cured at 150°C develops primarily linear structures initially with significant crosslinking/branching only at later stages of the reaction. Consider the schematic shown in Figure 17. Structure development in the sample cured at 150°C is likely similar to that shown in top scheme of Figure 17. This scheme shows the type of molecular network expected if the initial microgels develop a

linear architecture. Linear segments extend until they eventually connect at the gel point, then unreacted species crosslink within this existing linear network. This behavior in samples cured at 150°C is supported by the conversion plot shown in Figure 16b, where the initial high concentration of secondary amine indicates a mostly linear structure during the pre-gelation stage of cure while the majority of crosslinks form during the main stage of network growth. This type of network growth produces a more homogeneous network structure, as supported by the absence of nodular structures in Figure 23e. The bottom scheme of Figure 17 shows the type of molecular network architecture expected if the microgels develop linear segments and crosslinks nearly simultaneously. Crosslinked gels grow in size until they contact at the gel point, at which point chemical bonds are formed at the interface of individual structures. This type of network growth would be likely to produce non-homogenous network connectivity. This behavior is supported by the conversion plots shown in Figure 16a and 19c where branched or crosslinked segments within a sample are seen be created at similar rates.

The contradictory behavior of faster crosslink production at both lower and higher temperatures can be explained by considering the two different ways in which the reaction of the amine species is temperature dependent. As discussed previously, autocatalysis of the reaction is expected to be more important for the production of crosslinks as an adjacent hydroxyl moiety is available to stabilize the participating species during the reaction of the secondary amine. This effect will be more important at lower temperatures as hydrogen bonding is expected to be disrupted at higher curing temperatures. The production of crosslinks therefore, is encouraged at low reaction temperatures. Primary amines are more reactive than secondary amines. However, the

difference between reactivity is reduced at higher reaction temperatures.[47] The production of crosslinks, therefore, is also encouraged at high reaction temperatures. The difference between the rate of linear and crosslinked segment production is greatest at moderate reaction temperatures of around 150°C (see Table 2). This means that the conformational restriction caused by intramolecular crosslinking reactions that is predicted by Labana, Chompff and Newman to encourage the formation of a non-homogenous network architecture is minimized at moderate temperatures.

The fracture surfaces shown in Figure 23 reflect the differences in molecular connectivity that will result from these two different modes of molecular network development. The remnants of the initial crosslinked microgels can still be seen as the nodular morphology observed in Figures 23b and 23f. These samples did not form homogeneous networks, as evidenced by the regular, repeating higher crosslinked domains observed at the critical fracture manifold. While both figures show evidence of the nodular morphology, there are clear differences in the regularity and size of the nodular structures. One possible explanation for this is the increased contribution of the etherification reaction to molecular network formation that should be expected at the higher curing temperature of the sample shown in Figure 23f. Figure 23e shows little residual evidence of nodular regions of higher crosslink density in agreement with the structure analysis from NIR data. The increase in roughness indicates that the propagating crack tip now deviates strongly to follow the lowest-energy propagation pathway. The linear molecular growth of the initial microgels enables the formation of larger homogeneous domains in the network structure rather than the smaller, regularly spaced domains of relatively higher and lower crosslink density seen at the fracture

surface of samples cured at 90°C and 185°C (25b and 25f, respectively). This nanoscale difference in fracture behavior is reflected in bulk measurement of the fracture toughness.

Influence of Molecular Connectivity on Macroscopic Fracture Behavior

Fracture testing provides a way to gain an understanding of the interfacial connectivity of individual nanostructures. Figure 25a illustrates the resistance to fracture for a series of samples cured at different temperatures as determined by the fracture toughness. Each sample was cured to the onset of vitrification. Samples cured between 150°C and 185°C show the highest resistance to fracture while samples cured at 90°C show the lowest resistance to fracture. Samples cured at 50°C were so brittle that the fracture toughness was unmeasureable. Samples cured at 150°C show a more homogeneously connected network structure, as observed by AFM interrogation of the critical fracture manifold, and also higher fracture toughness. Samples cured at 90°C show a less homogeneously connected network structure, as observed by AFM interrogation of the critical fracture manifold, and lower fracture toughness. It must be noted, however, that due to the large differences in overall conversion of each sample it cannot be said that this result is solely due to differences in the distribution of crosslinks within the system as the total connectivity within the network is expected to be dramatically influenced by overall monomer conversion.

Postcuring the samples increases the resistance to fracture of low-temperature cured samples by increasing monomer conversion and therefore also the connectivity of their molecular networks. Samples cured at 90°C only underwent 84% epoxy conversion prior to gelation and also show the most heterogeneity in the network and lowest fracture toughness. The under-crosslinked internodular domain that serves as the low-energy

fracture pathway likely consists of high amounts of this unreacted material. Postcuring drives epoxy conversion of this sample to nearly 100% and this increased molecular connectivity is reflected in the large increase in fracture toughness shown in Figure 25b. Figure 26 shows topographic AFM images of a sample cured at 90°C with and without a postcuring treatment. The clear nodules observed in Figure 26a (no post-curing) are much less distinct after postcuring. Additionally, there is an indication that postcuring causes individual structures begin to coalesce into larger structures, such as the large structure seen at the right side of 29b. This is indicative of increased connectivity which causes the propagating crack tip to deviate around these new regions of relatively higher crosslink density.

Postcuring drove epoxy conversion to nearly 100% in all samples, regardless of initial cure temperature. Figure 25b shows similar fracture toughness values for each sample after postcuring (except for the sample initially cured at 200°C which visually appeared to have undergone thermal degradation during the postcuring treatment). Figure 25b shows that this appears to be a limiting value for the fracture toughness of fully cured systems as all samples (aside from the degraded 200°C sample) show nearly identical values at near 100% conversion, regardless of initial cure temperature. Samples cured at 150°C, 170°C and 185°C (with 84%, 88% and 94% epoxy conversion, respectively) show lower fracture toughness values after postcuring. This may be associated with a decrease in free volume associated with the increase in crosslink density that encourages brittle fracture propagation. Alternatively, it could be rooted in thermal degradation similar to what was observed for samples initially cured at 200°C.

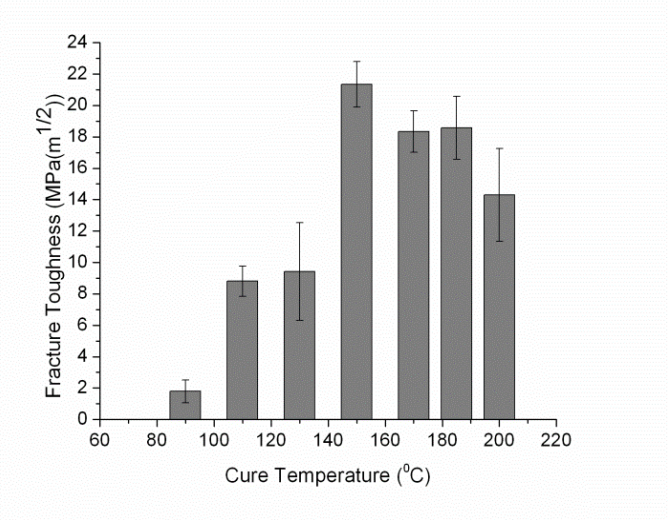

(a)

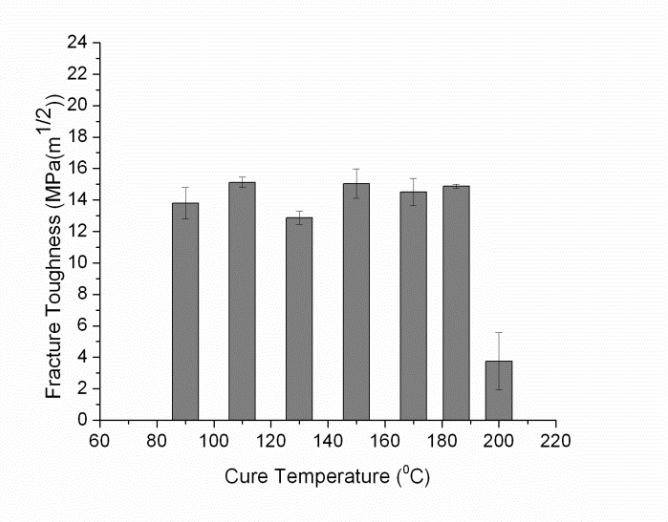

(b)

Figure 25. Fracture toughness of samples cured at different temperatures. (a) shows values for isothermally cured samples, (b) shows values for samples postcured at 200°C for 120 minutes.

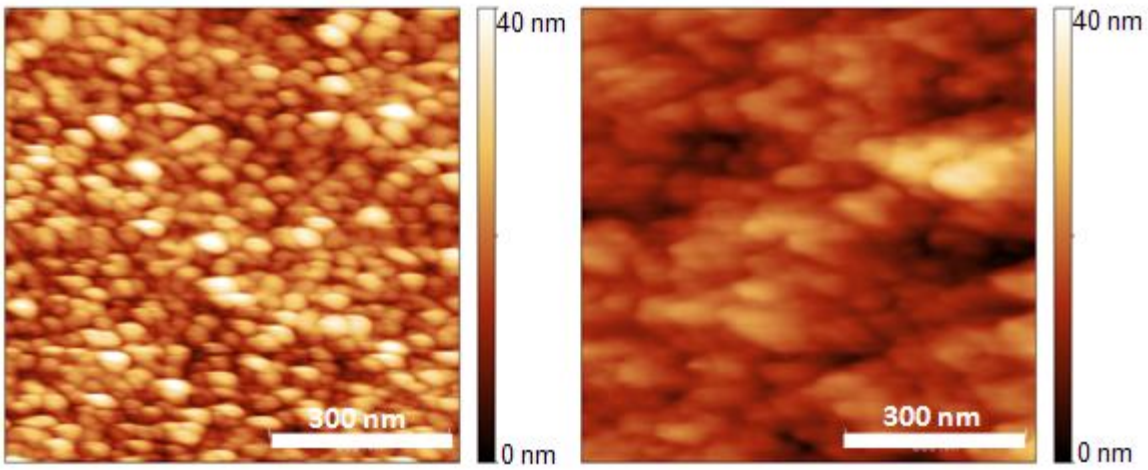

(a) (b)

Figure 26. Topographic AFM images of a sample cured at 90°C to the onset of vitrification (a) prior to postcure and (b) after postcuring at 200°C for 120 minutes.

Figure 27 shows topographic AFM images of a sample cured at 50°C before and after postcuring. Samples cured at this temperature vitrified before reaching the gel point, therefore, the image on the left shows the critical manifold of non-crosslinked material. Postcuring transformed the sample into an insoluble thermoset, indicating the formation of crosslinks. Some indication of substructure is possibly seen at the fracture surface after postcuring, however it is not nearly as distinct as the nodular morphology seen in other samples. This behavior provides further evidence that the underlying network structure can be tuned by controlling the reaction temperature. The postcuring process used here was a simple step-increase from 50°C to 200°C. It is likely that the vitrified sample melted prior to gelation. A more carefully programmed thermal cycle may allow a sample to gel from the solid state. It would be interesting to see the critical manifolds that result from this type of carefully controlled processing.

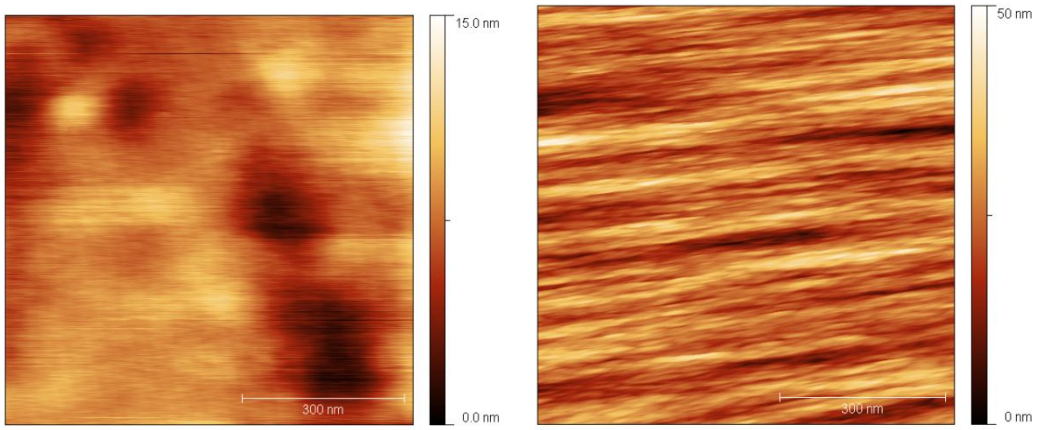

Figure 27. Topographic AFM images of a sample cured at 50°C. The left image shows the as-cured sample (RMS=2.0 nm) while the right image shows the sample after postcuring at 200°C for 120 minutes (RMS=6.3 nm).

CHAPTER IX

CONCLUSIONS

This work has investigated the development of the network architecture of an epoxy-amine thermoset typical of the resins used as the matrix material for high performance aerospace applications. Key findings of this research include:

1. The critical fracture manifold is a valuable tool for the elucidation of network structure in thermoset systems. The technique developed in this work utilized a propagating crack tip as a mesoscale "probe" coupled with fracture surface interrogation by atomic force microscopy in order to identify regions of the network with different relative levels of crosslink density.

2. The temperature-dependent reactivity ratio of the primary to secondary amine leads to different relative production rates of linear versus crosslinked molecular connections at different cure temperatures. It was determined that both lower and higher reaction temperatures favor the production of linear and crosslinked segments at similar rates as compared to the relative rate of production at moderate reaction temperatures. This seemingly odd behavior was explained by considering influence of autocatalytic behavior at lower temperatures and the similar reactivity ratio of the primary and secondary amine at higher temperatures.

3. Cured epoxy-amine molecular networks possess a heterogeneous network architecture. The commonly observed nodular morphology first appears at the gel point and the structures become more regular and distinct as the sample moves through the main stage of network growth. The nodular structure becomes less distinct after the onset of vitrification, likely due to increased internodular connectivity after extended cure time.

4. The temperature dependent behavior of the reaction of the amine with epoxy can be used to tune the architecture of the molecular network. Samples cured to the onset of vitrification at different temperatures were found to possess different morphologies of the critical fracture manifold.

5. The architecture developed during the initial stages of cure seems to become a permanent feature of the molecular network. Postcuring of the samples was seen to alter the critical fracture manifold. However, it did not cause all samples to take on a similar network architecture, as evidenced by the critical fracture manifold.

CHAPTER X

RECCOMENDATIONS FOR FUTURE WORK

The information gained from this work can be enhanced by a full investigation of the way observed differences in the network architecture influence macroscopic behavior. The characterization of fracture toughness presented here is promising, however, it was limited by the extreme brittleness of the samples. An investigation of influence of the mesoscale structure of the crosslinked molecular network on solvent transport properties would be especially interesting, especially if coupled with small angle neutron scattering similar to the work conducted by Gu.[66]

An investigation into the ability for more elaborate cure cycles to control the resulting network architecture would also be worthy of pursuit. The information obtained in this work has shown that it possible to tune the architecture of the crosslinked network by exploiting the temperature dependence of the epoxy/amine network building reaction. A careful control over network development will likely yield interesting and new controlled network architectures.

A similar investigation into other glassy thermoset polymers would provide valuable information about the mesoscale structure of other materials. This knowledge would be especially valuable to the aerospace and defense industry, especially if these studies were to be conducted on "next generation" composite matrices such as polybenzoxazines or cyanate esters.

This work has shown that the architecture of the crosslinked network could be passively controlled by adjusting the reaction temperature. The ability to *actively* control the architecture of the crosslinked network will most likely enable the creation of exotic

network architectures, for example, the production of networks with gradients in crosslink density or the controlled distribution of free volume within the crosslinked network. The production of this type of network will enhance the utilization of composite matrices by potentially enabling the crosslinked matrix to perform dual roles as both a structural member and also a moisture barrier, a sensor or as an energy storage device. These advancements may be possible if the introduction of thermal energy into the system were to be more precisely controlled. This direction will be pursued by the author as part of an upcoming postdoctoral position at the Air Force Research Laboratory.

REFERENCES

1. LeMay, J.; Kelley, F. *Adv. Polym. Sci.* **1986**, *78*, 115-148.

2. Askadskii, A. *Russ. Chem. Rev.* **1998**, *67*, 681-712 .

3. Dusek, K. *Adv. Polym. Sci.* **1986**, *78*, 1-59.

4. Seil, B. *Boeing Frontiers,* **2009**, *12*, 38-40.

5. Bicerano, J. *Prediction of Polymer Properties*, 2nd ed.; Marcel Dekker: New York, 1996.

6. Askadskii, A. *Physical Properties of Polymers: Prediction and Control*, Gordon and Breach: Amsterdam, 1996.

7. van Krevelen, D.; Nijenhuis, K. *Properties of Polymers*, 4th ed.; Elsevier: Amsterdam, 2009.

8. Allen, M.; Tildesley, D. *Computer Simulation of Liquids*, Oxford University Press: Oxford, 1987.

9. Jackson, M.; Kaushik, M.; Nazarenko, S.; Ward, S.; Maskell, R.; Wiggins, J. *Polymer* **2011**, *52*, 4528-4535.

10. Pyun, E.; Chong, S. *Macromolecules* **1991**, *24*, 855-861.

11. Tucker, S. *Ph.D. Thesis*, The University of Southern Mississippi, Hattiesburg, MS, 2010.

12. Meyer, F.; Sanz, G.; Eceiza, A.; Mondragon, I.; Mijovic, J. *Polymer* **1995**, *36*, 1407-1414.

13. Swanson, J. *Ph.D. Thesis*, The University of Southern Mississippi, Hattiesburg, MS, 2010.

14. Suarez, S.; Gibson, R.; Sun, C.; Chaturvedi, *S. Exp. Mech.* **1986**, *26*, 175-184.

15. Cirino, M.; Friedrich, K.; Pipes, R. *Wear* **1987**, *121*, 127-141.

16. Mallick, P. *Fiber-Reinforced Composites*, 3rd ed.; CRC Press: New York, 2007.

17. Norris, G.; Thomas, G. *Boeing 787 Dreamliner - Flying Redefined*, Aerospace Technical Publications: Perth, 2005.

18. Raytheon Corportaion, *Zumwalt Class Destroyer Integrated Composite Deckhouse & Apertures*. http://www.raytheon.com/capabilities/products/ddg_1000/tech/idha/index.html (January 10, 2012).

19. Acmite Market Intelligence. *World Epoxy Resin Market*. Acmite International: Ratingen, 2010.

20. Sahagun, C.; Morgan, S. *ACS Appl. Mater. Interfaces* **2012**, *4*, 564-572.

21. Sahagun, C.; Knauer, K.; Morgan, S. *J. Appl. Polym. Sci.* **2012**, *In Press*.

22. Ward, I. *Mechanical Properties of Solid Polymers*, 2nd ed.; John Wiley & Sons: Chichester, 1983.

23. Bueche, F. *Physical Properties of Polymers*, Interscience Publishers: New York, 1962.

24. Menard, K. *Dynamic Mechanical Analysis*, CRC Press: Boca Raton, 1999.

25. Ellis, B. *Chemistry and Technology of Epoxy Resins,* Blackie Academic & Professional: Glasgow, 1993.

26. Xu, L.; Fu, J.; Schlup, J. *J. Am. Chem. Soc.* **1994**, *116*, 2821-2826.

27. Smith, M.; March, J. *March's Advacned Organic Chemistry*, 5 ed.; John Wiley & Sons: New York, 2001.

28. Duchet, J.; Pascault, J. *J. Polym. Sci., Part B: Polym. Phys.* **2003**, *41*, 2422-2432.

29. Riccardi, C.; Williams, R. *J. Appl. Polym. Sci.* **1986**, *32*, 3445-3456.

30. Lan, T.; Kaviratna, P.; Pinnavaia, T. *J. Phys. Chem. Solids* **1996**, *57*, 1005-1010.

31. Riccardi, C.; Adabbo, H.; Williams, R. *J. Appl. Polym. Sci.* **1984**, *29*, 2481-2492.

32. Min, B.; Stachurski, Z.; Hodgkin, J. *Polymer* **1993**, *34*, 4488-4495.

33. Kozielski, K.; George, G.; St. John, N.; Billingham, N. *High Perform. Polym.* **1994**, *6*, 263-286.

34. Mijovic, J.; Wijaya, J. *Polymer* **1994**, *35*, 2683-2686.

35. Xu, L.; Schlup, J. *J. Appl. Polym. Sci.* **1998**, *67*, 895-901.

36. Schechter, L.; Wynstra, J.; Kurkjy, R. *Ind. Eng. Chem.* **1956**, *48*, 94-97.

37. Min, B.; Stachurski, Z.; Hodgkin, J.; Heath, G. *Polymer* **1993**, *34*, 3620-3627.

38. Riccardi, C.; Williams, R. *J. Appl. Polym. Sci.* **1986**, *32*, 3445-3456.

39. Fryauf, K.; Strehmel, V.; Fedtke, M. *Polymer* **1993**, *34*, 323-327.

40. Rozenberg, B. *Adv. Polym. Sci.* **1986**, *75*, 113-165.

41. Mijovic, J.; Andjelic, S. *Macromolecules* **1995**, *28*, 2787-2796.

42. Horie, H.; Hiura, H.; Sawada, M.; Mita, I.; Kambe, H. *J. Polym. Sci.* **1979**, *A1.8*, 1357-1372.

43. Sourour, S.; Kamal, M. *Thermochim. Acta* **1976**, *14*, 41-59.

44. Camargo, R.; Gonzalez,V.; Macosko, C. *Rubber Chem. Technol.* **1983**, *56*, 774-778.

45. Macosko, C. *Br. Polym. J.* **1985**, *17*, 239-245.

46. Barton, J. *Adv. Polym. Sci.* **1985**, *72*, 111-154.

47. Wang, X.; Gillham, J. *J. Appl. Polym. Sci.* **1991**, *43*, 2267-2277.

48. Halley, P.; George, G. *Chemorheology of Polymers*, Cambridge University Press: Cambridge, 2009.

49. Enns, J.; Gillham, J. *J. Appl. Polym. Sci.* **1983**, *28*, 2567-2591.

50. Peng, X.; Gilham, J. *J. Appl. Polym. Sci.* **1985**, *30*, 4685-4696.

51. Odian, G. *Principles of Polymerization*, 4th ed.: John Wiley & Sons: Hoboken, 2004.

52. Carothers, W. *Trans. Faraday Soc.* **1936**, *32*, 39-49.

53. Flory, P. *J. Am. Chem. Soc.* **1941**, *63*, 3083-3090.

54. Stockmayer, W. *J. Chem. Phys.* **1943**, *11*, 45-56.

55. Carothers, W. *Trans. Faraday Soc.* **1936**, *32,* 39-49.

56. Labana, S.; Newman, S.; Chompff, A. *Polymer Networks: Structural and Mechanical Properties*, Plenum: New York, 1971.

57. Bueche, F.; Cashin, W.; Debye, P. *J. Chem. Phys.* **1952**, *20*, 1956-1959.

58. Zimm, B.; Stockmayer, W. *J. Chem. Phys.* **1949**, *17*, 1301-1313.

59. Feng, J.; Berger, K.; Douglas, E. *J. Mater. Sci.* **2004**, *39*, 3413-3424.

60. Levita, G.; De Petris, S.; Marchetti, A.; Lazzeri, A. *J. Mater. Sci.* **1991**, *26*, 2348-2352.

61. Escher, U. *Cryogenics* **1995**, *35*, 775-778.

62. Erath, E.; Spurr, R. *J. Polym. Sci.* **1959**, *35*, 391-399.

63. Racich, J.; Koutsky, J. *J. Appl. Polym. Sci.* **1976**, *20*, 2111-2129.

64. Mijovic, J.; Koutsky, J. *Polymer* **1979**, *20*, 1095-1107.

65. Morgan, R.; O'Neal, J. *J. Mater. Sci.* **1977**, *12*, 1966-1980.

66. Gu, X.; Nguyen, T.; Ho, D.; Oudina, M.; Martin, D.; Kidah, B.; Jasmin, J.; Rezig, A.; Sung, L.; Byrd, E.; Jean, Y.; Martin, J. *J. Coat. Technol. Res.* **2005**, *2*, 547-556.

67. Matyi, R.; Uhlmann, D. *J. Polym. Sci., Polym. Phys. Ed.* **1980**, *18*, 1053-1063.

68. Mijovic, J.; Tsay, L. *Polymer* **1980**, *22*, 902-906.

69. Gu, X.; Sung, D.; VanLandingham, M.; Nguyen, T. *Proc. Mater. Res. Soc.* **2001**, 710, DD10.9.1.

70. Kishi, H.; Naitou, T.; Matsuda, S.; Murakami, A.; Muraji, Y.; Nakagawa, Y. *J. Polym. Sci., Part B: Polym. Phys.* **2007**, *45*, 1425-1434.

71. Kreibich, U.; Schmid, R. *J. Polym. Sci.* **1975**, *53*, 177-185.

72. Dusek, K.; Plestil, J.; Lednicky, F.; Lunak, S. *Polymer* **1978**, *19*, 393-397.

73. Dusek, K. *Angew. Makromol. Chem.* **1996**, *240*, 1-15.

74. Sherman, C.; Zeigler, R.; Verghese, N.; Marks, M. *Polymer* **2008**, *49*, 1164-1172.

75. Paluch, M. *J. Phys.: Condens. Matter* **2000**, *12*, 9511-9524.

76. Oleinik, E. *Adv. Polym. Sci.* **1986**, *80*, 49-99.

77. Mijovic, J.; Koutsky, J. *J. Appl. Polym. Sci.* **1979**, *23*, 1037-1042.

78. Bell, J. *J. Appl. Polym. Sci.* **1982**, *27*, 3503-3511.

79. VanLandingham, M.; Eduljee, R.; Gillespie, W. *J. Appl. Polym. Sci.* **1998**, *71*, 699-712.

80. Griffith, A. *Philos. Trans. R. Soc. London Series A.* **1921**, *221*, 163-198.

81. Kinloch, A. *Adv. Polym. Sci.* **1985**, *72*, 45-67.

82. Houwink, R. *Trans. Faraday Soc.* **1936**, *32*, 131-143.

83. Kausch, H. *Polymer Fracture*, Springer-Verlag: Berlin, 1978.

84. McClintock, F.; Irwin, G. *Plasticity Aspects of Fracture Mechanics*, The American Society for Testing and Materials: Chicago, 1965.

85. Holm, E.; Duxbury, P. *Scr. Mater.* **2006**, *54*, 1035-1040.

86. Holm, H.; Meinke, H.; McGarrity, E.; Duxbury, P. *Mater. Sci. Forum* **2004**, *467-470*, 1039-1044.

87. Holm, E.; McGovney, G. *Microscale Modeling and Simulation*, Sandia National Laboratories: Albuquerque, 2000.

88. Holm, E.; McGovney, G. *Minimum Surface Formation Energy for Three-Dimensional Intergranular Fracture,* Sandia National Laboratories: Albuquerque, 1999.

89. Holm, E. *J. Am. Ceram. Soc.* **1998**, *81*, 455-459.

90. Gogolewski, S. *Polymer* **1977**, *18*, 647-653.

91. Friedrich, K. *Ph.D. Dissertation*. Ruhr-Universitat Bochum, 1978.

92. Franck, A. *Measuring and Evaluationg Oscillation Data,*TA Instruments: New Castle, 2008.

93. Chambon, F.; Winter, H. *J. Rheol.* **1987**, *31*, 683-697.

94. Winter, H.; Chambon, F. *J. Rheol.* **1986**, *30*, 367-382.

95. Pramanik, M.; Swanson, J.; Scott, J.; Mendon, S.; Rawlins, J. *Presented at SAMPE 41st ISTC,* SAMPE: Witchita, 2009.

96. ASTM International, *ASTM D5045,* ASTM International: West Conshohocken, 1995.

97. The American Society of Mechanical Engineers, *ASME B46.1-1995,* ASME: New York, 1995.

98. Pharr, G.; Oliver, W.; Brotzen, F. *J. Mater. Res*. **1992**, *7*, 613-617.

99. Tung, C.; Dynes, P. *J. Appl. Polym. Sci.* **1982**, *27*, 569-574.

100. Holly, E.; Venkataraman, S.; Chambon, F.; Winter, H. *J. Non-Newtonian Fluid Mech.* **1988**, *27*, 17-26.

101. Kim, D.; Kim, S. *Polym. Bull.* **1987**, *18*, 533-539.

102. Assche, G.; Hemelrijck, A.; Rahier, H.; Mele, B. *Thermochim. Acta* **1995**, *268*, 121-142.

103. George, G.; Cole-Clarke, P.; St John, N.; Friend, G. *J. Appl. Polym. Sci.* **1991**, *42*, 643-657.

104. Musto, P.; Ragosta, G.; Mascia, L. *Chem. Mater.* **2000**, *12*, 1331-1341.

105. Chike, K.; Myrick, M.; Lyon, R.; Angel, S. *Appl. Spectrosc.* **1993**, *10*, 1631-1635.

106. Magonov, S.; Elings, V.; Whangbo, M. *Surf. Sci.* **1997**, *375*, L385-L391.

107. McLean, R.; Sauer, B. *Macromolecules* **1997**, *30*, 8314-8317.